Unsettling the settled: Simple musings on the complex climatic system

Demetris Koutsoyiannis*, George Tsakalias

Department of Water Resources and Environmental Engineering, School of Civil Engineering, National Technical University of Athens Heroon Polytechneiou 5, 157 80 Zographou, Greece

*** Correspondence:**
Corresponding Author, dk@itia.ntua.gr

Keywords: climate; climatic system; atmosphere; thermodynamics; greenhouse.

Abstract

Our revisit of fundamental issues of climate challenges the notion and term of the "greenhouse effect", and attempts a scientific reevaluation using minimal assumptions, such as Newton's laws, maximum entropy and gas spectroscopy. It replaces terms like "greenhouse gas" with "radiatively active gas" (RAG) and "greenhouse effect" with "atmospheric radiative effect" (ARE). While ARE exists in several planets' atmospheres, on Earth it is primarily driven by water vapor and clouds, with CO_2 playing a minor role (especially anthropogenic CO_2 which represents 4% of total emissions). Equilibrium thermodynamics, via entropy maximization or molecular collision simulation, leads to an isothermal atmosphere at about 250 K (the average temperature of the troposphere and stratosphere) irrespective of RAG presence or not. It is the troposphere's 6.5 K/km temperature gradient, partly shaped by moist adiabatic processes, that drives the atmosphere away from this equilibrium and warms the surface to about 288 K on average, with ARE (mainly water vapor and clouds) contributing to the warming, but only when this gradient exists. The temperature gradient varies spatially and temporally and, since 1950, has weakened in the tropics and grown in the polar areas, resulting in a decrease of the surface equator-to-pole gradient, as expected in global warming conditions.

Dedicated to the memory of Anna (Annouska) Patrikiou – Koutsoyiannis
who left this world while this research was conducted

The climate alarm establishment is some combination of a religious cult and organized crime
(William Happer; https://www.youtube.com/watch?v=PblYr-KjOVY and personal communication)

1 Introduction

Do we live in a greenhouse? Most people would give an affirmative reply given the enormous campaign to promote the climate agenda that is founded on the concepts of greenhouse gases (GHG) and greenhouse effect (GHE). Systematic searches in Google Books (https://books.google.com/ngrams/) and Internet Archive (https://archive.org/) show that, while the term 'greenhouse' is old (already appearing in the 18^{th} century with its literal meaning), the terms GHG and GHE are newer. GHE was first used in 1960s by NASA in relation to planetary atmospheres (Samuelson, 1965; Wildt, 1965). Since the late 1970s, however, the usage of GHE has changed to closely associate it with carbon dioxide (CO_2) and its emission into the atmosphere from the burning of fossil fuels, but also to imply that this causes disastrous disastrous effects on climate, economy and every aspect of life (Murray, 1979; Bernard Jr, 1980; EXXON, 1982; Gribbin, 1982;

Barth and Titus, 1984; U.S. House of Representatives, 1984; Bolin et al. 1986, Gay, 1986). Notably, these developments followed politically driven alerts about climate and, arguably, the entire climate narrative does not have a geophysical origin but a political one (Lindzen, 2020; Koutsoyiannis, 2021) with ideological connotations (cf. the epigram at the beginning of this paper).

If we adhere to science and follow the scientific method, it becomes important to clarify the concepts we use (cf. the Aristotelian notion of sapheneia; Koutsoyiannis, 2024a) and in this case the reply to the above question would be negative: we do not live in a greenhouse. A simple revisit of the definition of a greenhouse (a structure that is designed to regulate the temperature and humidity of the environment inside) suffices to see that the Earth's atmosphere is not a greenhouse, even though effects such as those that the term GHE purports to describe are present on Earth, as well as on other planets in the solar system that have an atmosphere (see section 3.2).

For scientific clarity and accuracy, here we replace the term GHG with *radiatively active gas* (RAG), comprising water vapor (WV) and non-condensing radiatively active gases (NC RAG). Also, we replace the term GHE with *atmospheric radiative effect* (ARE). ARE is the influence of RAGs on the energy balance in the atmosphere by absorbing, emitting, and scattering radiation across both shortwave (SW) and longwave (LW) spectra. These processes influence the flow of energy between the Earth's surface, the atmosphere, and space. While the term GHE is often associated primarily with heat-trapping, ARE explicitly recognizes all radiative interactions in the atmosphere. It avoids the misleading analogy of a greenhouse and is more applicable to a scientific framework that considers both SW and LW radiation.

It is also important to note that WV and clouds (for which WV is responsible) represent the overwhelmingly greater part of the ARE, while CO_2 represents 4%-5%. Also, human CO_2 emissions are a mere 4% of the total, with the vast majority (96%) being natural. Furthermore, the causal link of temperature and CO_2 is the reverse of that commonly assumed. That is, the changes in temperature cause those in CO_2 concentration and not the other way around. All these have been documented in recent publications summarized in Koutsoyiannis (2024c) and in an AI-chatbot led review paper by Grok 3 beta et al. (2025). These developments contradict the established "climate science", which is regarded as settled, particularly with respect to the CO_2 and the human contribution to the increase of its atmospheric concentration in the last decades. However, science can never be settled, particularly the so called "climate science" which purports to deal with one of the most complex systems on Earth, the climatic system (cf. Koonin, 2021). It is recalled that the climatic system consists of the atmosphere, the hydrosphere (including its solid phase—the cryosphere), the lithosphere and the biosphere, which mutually interact and respond to external influences (system inputs).

It is thus healthy to question whether the fundamental ideas about climate correspond to reality, leaving aside the fact that they are established or settled. In this respect, this paper examines (in section 3) the following fundamental questions, without the preconception of standard answers.

1. Is there an empirically verified ARE in the atmosphere?
2. What would be the atmospheric temperature profile in equilibrium?
3. What is the empirically observed temperature profile, and does it differ from the equilibrium profile?
4. Is the ARE responsible for the observed temperature profile in the atmosphere?
5. What factors can explain the observed temperature profile?
6. What is the relative importance of ARE and temperature gradient in climate dynamics?
7. What are the recent changes in the atmospheric temperature gradient?

Note that the terms "temperature gradient" or simply "gradient" are used above and below as shortcuts for "(minus) vertical gradient of temperature in the troposphere" (also known as "lapse rate"). Whenever a different gradient direction is assumed, we specify it (e.g., surface equator-to-pole temperature gradient).

2 Data and software

The temperature data used here are taken from the ERA5 Reanalysis on a monthly scale. ERA5 stands for the fifth generation atmospheric reanalysis of the European Centre for Medium-Range Weather Forecasts (ECMWF; ECMWF ReAnalysis). Its data are publicly available for the period 1940 onwards at a spatial resolution of 0.5°. The data sets used here were retrieved from the Physical Sciences Laboratory platform of the US National Oceanic and Atmospheric Administration (NOAA) (WRIT: Monthly Timeseries: NOAA Physical Sciences Laboratory, https://psl.noaa.gov/cgi-bin/data/atmoswrit/timeseries.pl). For the period 1950 onwards, they are also accessible from the Climate Explorer platform (https://climexp.knmi.nl/) which in addition allows extended processing of the data.

Radiation data from satellites were retrieved from NASA's ongoing project Clouds and the Earth's Radiant Energy System (CERES, 2021) from the Terra platform (operational since January 2001). The specific product used here is the CERES SSF1deg monthly averaged TOA LW radiative fluxes at a 1°-regional grid, constant-meteorology-temporally-interpolated. The top-of-atmosphere (TOA) fluxes are provided for clear-sky and all-sky conditions and are available online.

The main software tool used here is RRTM (standing for rapid radiative transfer model), a hybrid physical/statistical approximation of the full line-by-line models, developed for climate studies. Its results have been extensively evaluated and rigorously validated (Mlawer et al., 1997). The model implementation used here is an interactive web application hosted by the University of Chicago (https://climatemodels.uchicago.edu/rrtm/) that simulates the radiation flux through Earth's atmosphere at a range of altitudes, calculating both SW (incoming and reflected sunlight) and LW (emitted by the ground and atmosphere), both upward and downward. Users can adjust parameters such as solar input, albedo, and atmospheric composition in order to study their effects on Earth's energy balance, revealing whether the planet gains or loses energy and enabling the parameters that lead to energy balance to be found.

Additional software was developed in-house to simulate the thermal equilibrium dynamics of a gas and to determine the altitude-dependent distribution of air density and temperature under gravity. The simulation is based solely on molecular collisions treated as perfectly elastic hard-sphere interactions, without any assumptions beyond Newton's laws. A detailed description is provided in Appendix C, and the software is available online as Supplementary Information, allowing interested readers to review the code, replicate the calculations, or simply view the simulation videos.

3 Analysis of questions

3.1 Is there an empirically verified ARE in the atmosphere?

The reply to this question is definitely affirmative and is based on observations. As noted by Ångström (1915), a pioneer of the measurement and modelling of radiation, the first observations relating to the problem of Earth's (LW) radiation to space were made between the years 1780 and 1850. Ångström (1915, p. 16) cites some sporadic measurements by several researchers for the period 1887-1912. From these measurements and from experiments in the 19th century, it was understood that the major constituents of the atmosphere, i.e., nitrogen (N_2) and oxygen (O_2), are transparent to LW radiation. In contrast, some minor constituents, particularly WV, carbon dioxide (CO_2) and ozone (O_3), absorb and reemit LW radiation, thus being RAG. John Tyndall (1865) pioneered our understanding of the dominance of WV in this process, of the importance of its presence for climate and life, and of the minor contribution of CO_2 in the ARE.

Ångström (1915, p. 16) provided his own systematic measurements, as well as a rough quantification of ARE in the following way:

> a surface at 15° C temperature ought to radiate 0.526 cal. If the observed effective radiation does not amount to more, for instance, than 0.15 cal, this must depend upon the fact that 0.376 cal is radiated to the surface from some other source of radiation. In the case of the earth this other source of radiation is probably to a large extent its own atmosphere.

Since the introduction of Penman's (1948) celebrated equation for natural evaporation from open water, the quantification of the ARE has become part of the routine hydrological calculations for real-world problems, such as those of the hydrological balance (of which evaporation represents a substantial component) and the irrigation needs in agricultural applications. Penman's (1948) equation is based on the presence of WV in the atmosphere and disregards that of NC RAG such as CO_2. A recent study by Koutsoyiannis and Vournas (2024) analyzed a large set of measurements distributed in time across a century, in which CO_2 has escalated from 300 to about 420 ppm. They concluded that the observed increase of the atmospheric CO_2 concentration has not altered the ARE in any discernible way. Thus, the ARE continues to be dominated by the quantity of WV in the atmosphere and CO_2 remains insignificant in the ARE.

Since the 1960s, detailed spectroscopic studies of RAGs were conducted, initially developed for military purposes and subsequently expanded to cover broader scientific use, evolving into an essential tool for atmospheric and astrophysical research. The results of these studies were compiled into HITRAN (High-Resolution Transmission), a molecular spectroscopic database designed to support the study of electromagnetic transmission and emission in gaseous media (McClatchey et al., 1973; Rothman et al., 1987; Goldman et al., 1988; Gordon et al., 2022). The database includes detailed line-by-line spectroscopic parameters for various molecular species.

Empirical data for testing the applicability of the theory have been provided early by Hanel and Conrath (1970) based on a Michaelson interferometer in a satellite. Recently, van Wijngaarden and Happer (2023, 2025) using these data showed that theory is impressively consistent with the observations, as shown in Figure 1, reproduced from the latter publications.

Some discrepancy appears in the Antarctica case, as the observed radiation is higher than that emitted by the Earth's surface. The explanation given by van Wijngaarden and Happer (2023, 2025) is this:

> Radiative forcing is negative over wintertime Antarctica since the relatively warm greenhouse gases in the troposphere, mostly CO_2, O_3 and H_2O radiate more to space than the cold ice surface at a temperature of T = 190 K, could radiate through a transparent atmosphere.

We note though that the T = 190 K, as well as the entire atmospheric profile, are estimated, rather than observed. Hanel and Conrath (1970) mention that

> no radiosonde data are available for comparison […] The profile can be anticipated intuitively from an examination of the spectrum […] The cold surface temperature results in the relatively low radiances found in the window region and between the water vapour lines.

Further examination of systematic ground temperature observations in the area shows that the assumed value of T = 190 K is unlikely. Specifically in the South Pole (station Amundsen-Scot; coordinates: 90°S, 0°E, prob: 2770 m), the lowest daily temperature in April 1970 (the month of the experiment) did not fall below 204K. The Vostok station (coordinates: 78.45°S, 106.87°E, 3420.0 m or prob: 3468 m) is the location with the lowest temperatures among 41 GHCN-D stations in Antarctica, and its temperatures in April are, on average, 7 K lower than in Amundsen-Scot. Furthermore, the reconstructed vertical temperature profile given by Hanel and Conrath (1970) does not seem plausible as it has an abrupt increase of >30 K at the level of 700 hPa. On the other hand, the ERA5 Reanalysis data suggest that there is a permanent state of temperature inversion (increasing temperature with increased altitude) between the atmospheric levels of 700 and 600 hPa (Figure 2), albeit not that big. This partly explains the discrepancy seen in Figure 1.

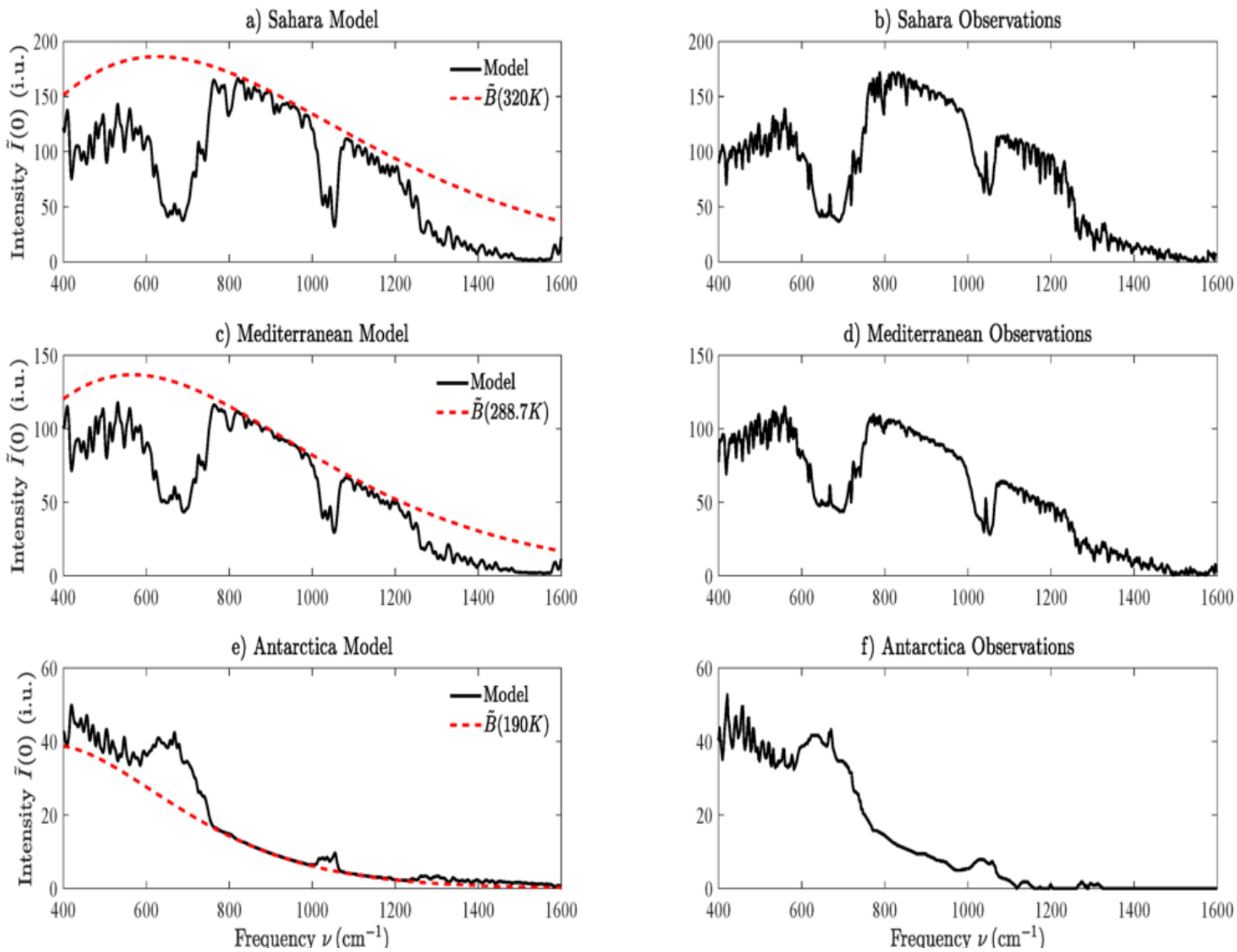

Figure 1 Reproduction of Figure 9 in van Wijngaarden and Happer (2025) (or Figure 10 in van Wijngaarden and Happer, 2023): Vertical intensities $\bar{I}(0)$ at the top of the atmosphere observed with a Michaelson interferometer in a satellite (Hanel and Conrath, 1970), and modeled with radiation transfer theory for the Sahara desert, Mediterranean and Antarctica. The intensity unit is 1 i.u. = 1 mW m^{-1} cm sr^{-1}.

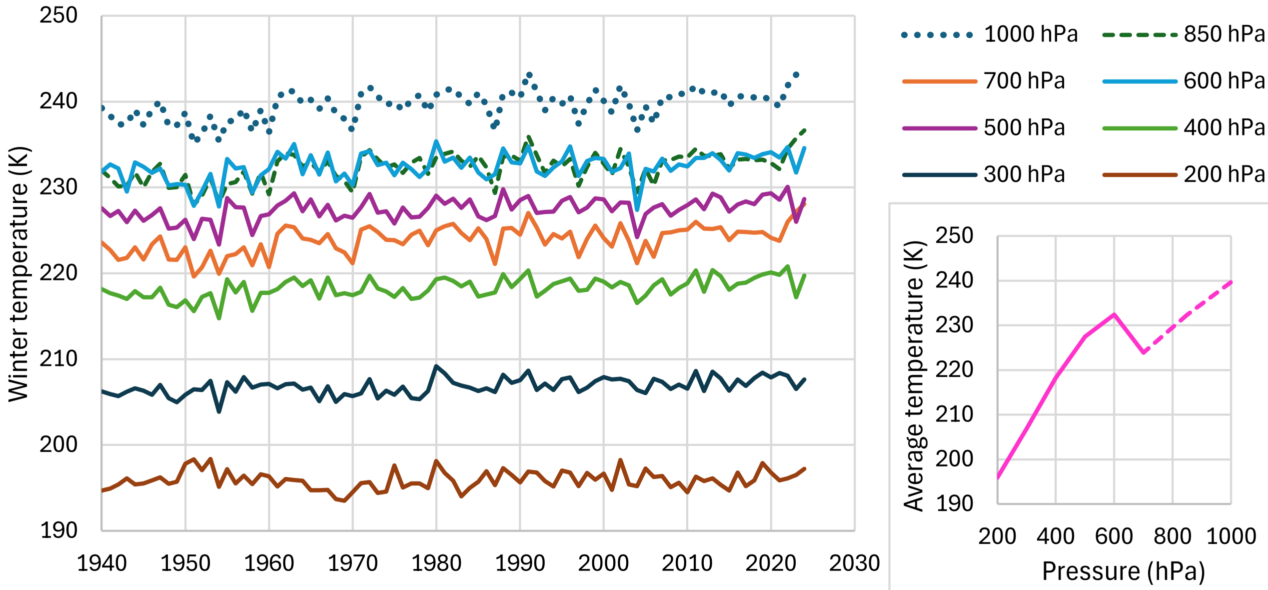

Figure 2 Evolution of mean monthly air temperature at the South Pole for the winter month that it is minimized at the indicated levels of the atmosphere. The inset on the right shows the average temperature vs. atmospheric pressure highlighting the inversion at pressure levels between 700 and 600 hPa. The pressure levels higher than 700 hPa (curves plotted as dashed lines) are not real as the altitudes are about 3000 m, corresponding to about 700 hPa. Data from ERA5 Reanalysis retrieved through NOAA's WRIT.

3.2 What would be the atmospheric temperature profile in equilibrium?

According to van Wijngaarden and Happer (2023), in the absence of greenhouse gases, an isothermal atmosphere would emerge and would not change with time. They also assert that a thermally isolated adiabatic atmosphere would slowly evolve into an isothermal atmosphere because of conductive heat flow from the warmer lower atmosphere to the colder upper atmosphere. Here we examine these statements with a slightly different formulation as seen in the question in the heading of this subsection.

It is well known that a gas in equilibrium tends to become isothermal, but here we examine the question also including gravity in the analysis. In fact, this problem is very old and is known as the Loschmidt paradox after Loschmidt (1876) who asserted that gravity could counteract the temperature uniformity implied by the second law as the kinetic energy of the molecules of a gas should be lower at higher elevation in compensation for the higher potential energy. The paradox puzzled many for years, yet both James Clerk Maxwell and Ludwig Boltzmann reacted negatively, supporting the isothermal hypothesis, as detailed in a recent analysis by Darrigol (2021).

Nonetheless, we deemed it useful to perform our own investigation in reply to this question independently of past arguments and using two methods. First, we maximize the entropy of a single molecule which is in motion in a vertical column under gravity. The single-molecule method has been successfully used before to derive the Clausius-Clapeyron equation (Koutsoyiannis, 2014). The development and application of the method to a spherical monoatomic and to a diatomic molecule are presented in Appendices A and B, respectively. In brief, the thermal (internal) energy per molecule turns out to be the same for all altitudes, equal to $\varepsilon_\theta = \beta\varepsilon/(\beta + 2)$, where β is the number of degrees of freedom of a molecule and ε is its total energy. This results in $3\varepsilon/5$ for monoatomic molecules and $5\varepsilon/7$ for diatomic molecules. The remaining energy $\varepsilon_g = 2\varepsilon/(\beta + 2)$ is the average dynamic energy due to gravity. The temperature is also constant, independent of the altitude, equal to

$$T = \frac{2\varepsilon_\theta}{\beta k} = \frac{2\varepsilon}{(\beta + 2)k} \tag{1}$$

where k is the Boltzmann constant. In other words, entropy maximization results in an isothermal atmosphere.

The same result emerges when we approach the problem with our second method, without invoking the principle of maximum entropy—by instead simulating the motion of molecules, modeled as perfectly elastic hard spheres, using only Newton's laws. Once again, the temperature is found to remain constant with altitude, as shown Figure 3 and discussed in detail in Appendix C. In other words, none of the approaches predicts a decrease in temperature with altitude, which is the observed behavior as will be explained in section 3.3.

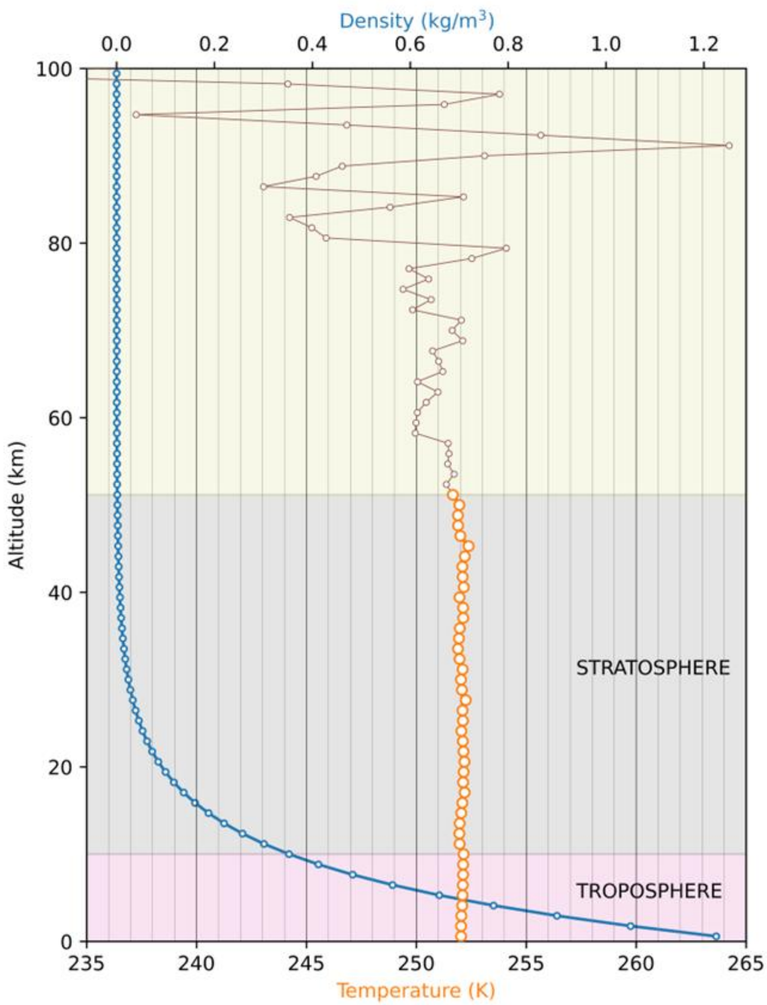

Figure 3 Reconstruction of the atmosphere's density and temperature profile, based on the molecular dynamics simulation results. Simulation consisted of 100 000 gas molecules, doing 1.2 billion collisions within a periodic box with reflective bottom boundary. The fluctuations at high altitudes are deemed as statistical effects due to small samples.

3.3 What is the empirically observed temperature profile, and does it differ from the equilibrium profile?

It is common knowledge that Earth's atmosphere is not isothermal. The temperature decreases with altitude in the troposphere, then it remains constant in the lowest layer of the stratosphere and continues to change at even higher altitudes. The typical atmospheric temperature profile is represented by the standard atmosphere adopted by the International Civil Aviation Organization (ICAO, 1993). According to the U.S. Standard Atmosphere (1976), the standard atmosphere is "A hypothetical vertical distribution of atmospheric temperature, pressure and density which, by international agreement, is roughly representative of year-round, midlatitude conditions." It is based on large inventories of observational data and is widely used for meteorological and engineering applications. The vertical profile of temperature vs. altitude and atmospheric pressure is shown in Figure 4, with the ground temperature being 15 °C or 288.15 K, and the gradient in the troposphere $\Gamma \coloneqq -\mathrm{d}T/\mathrm{d}z$ being 6.5 K/km up to the altitude of 11 km, taking a constant value of 216.65 K above this up to 20 km.

Clearly, the standard atmosphere is far from isothermal. Here we extensively use the standard atmosphere as satisfactorily representing reality, even though newer data and research (Wiencke, 2021) support slightly lower values of Γ, particularly at high latitudes. It is interesting to note that the average temperature in the standard atmosphere, calculated from the coordinates of Figure 4, is

$$\overline{T} = \frac{\int_0^\infty T(z)\rho(z)\mathrm{d}z}{\int_0^\infty \rho(z)\mathrm{d}z} = 250\ \mathrm{K}\ (= -23\ °\mathrm{C}) \tag{2}$$

where, by the ideal gases law, the air density ρ is proportional to p/T, with p denoting air pressure.

Figure 5 shows that temperature gradients appear in other planets and satellites in our solar system, and even in extrasolar planets (for additional rocky exoplanets see also Malik et al., 2019). In other words, isothermal atmospheres never seem to actually exist in planets.

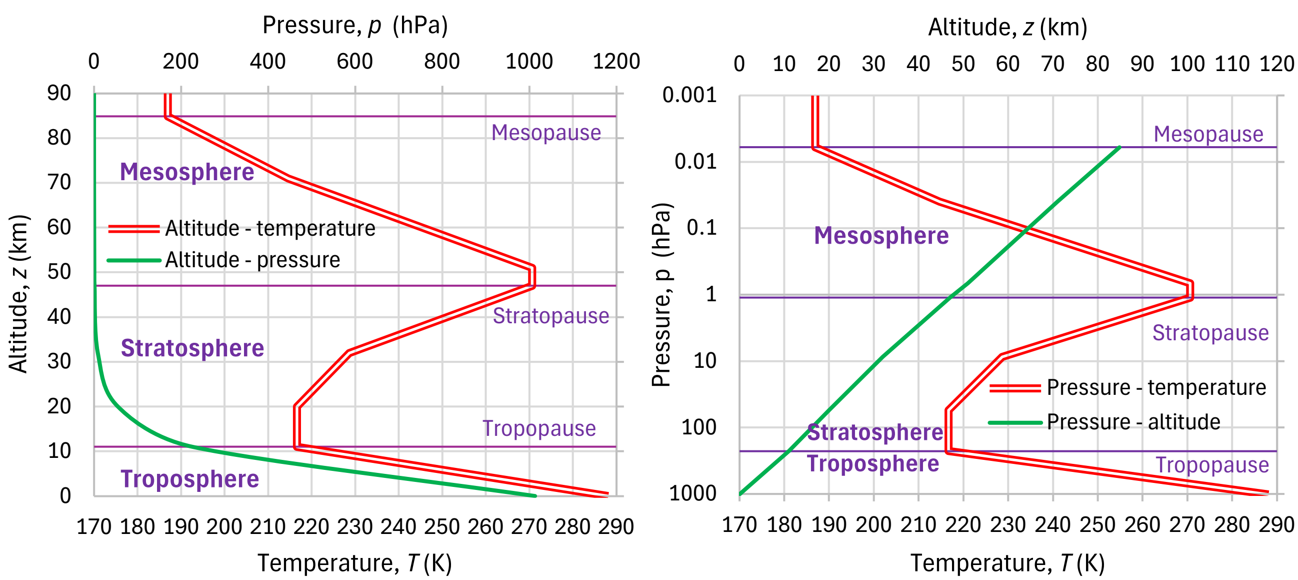

Figure 4 Vertical profiles of the ICAO (1993) standard atmosphere: (**left**) temperature and pressure as functions of altitude; (**right**) temperature and altitude as functions of pressure.

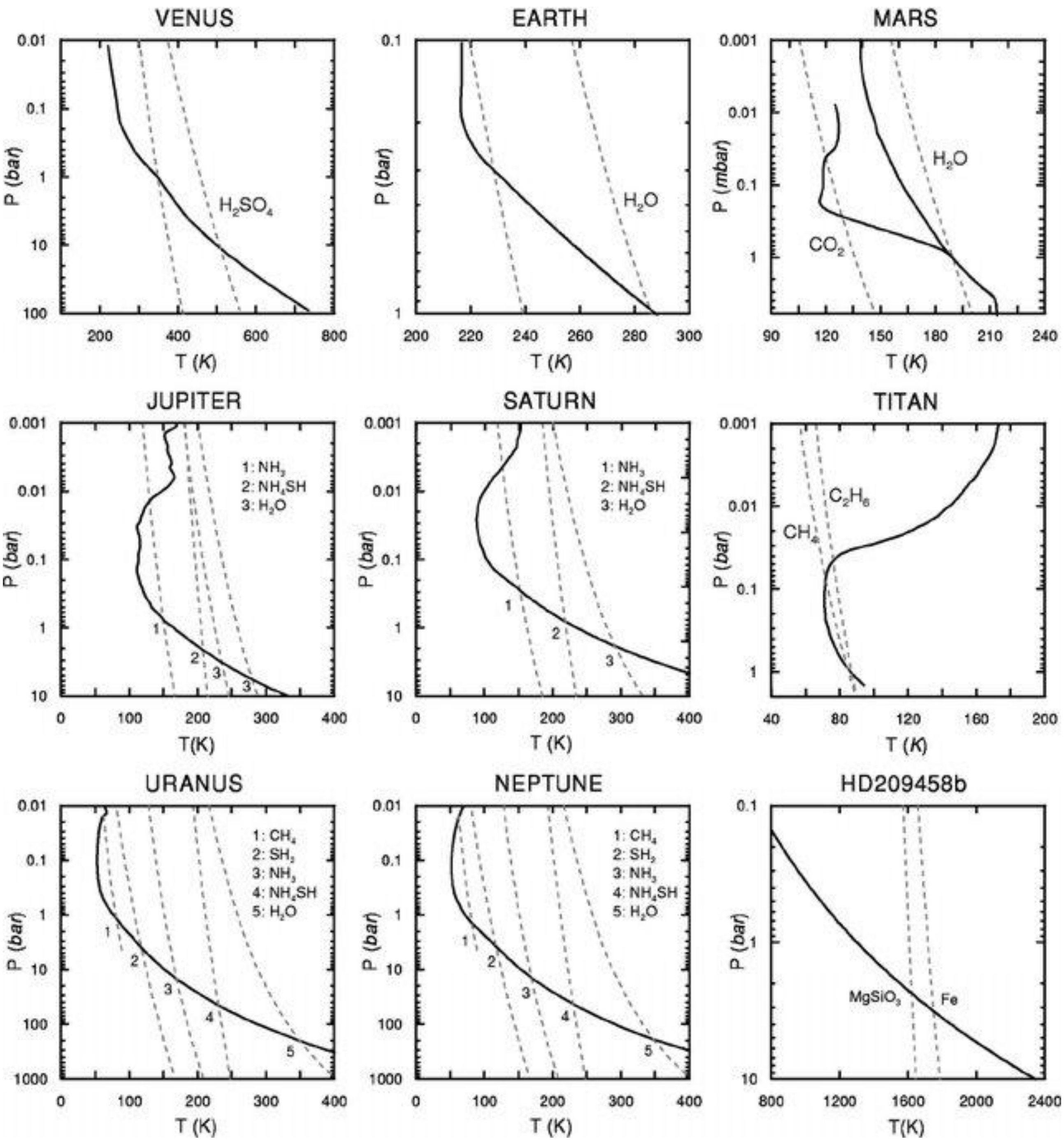

Figure 5 Vertical temperature profiles in the atmospheres of the indicated planets, the satellite Titan, and the extrasolar planet HD209458b (continuous lines), reproduced from Sánchez-Lavega et al. (2004, Fig. 3) with the permission of AIP Publishing. Saturation vapor pressure curves for the indicated condensates (substances forming clouds) for each planet are also plotted (dashed lines), details of which are given in the original publication.

Another important case, additional to the isothermal, is the isentropic atmosphere, where the per-molecule entropy is constant, independent of altitude. Following van Wijngaarden and Happer (2023) here we use the adjectives adiabatic and isentropic interchangeably, even though under some conditions, adiabatic processes can differ from isentropic processes. It is well known that in the absence of water vapor (dry conditions) the atmosphere has a constant temperature gradient equal to

$$\Gamma_{\mathrm{d}} = \frac{g}{c_{pd}} = 9.8 \text{ K/km} \tag{3}$$

where $g = 9.81$ m/s is the gravity acceleration (typical value for the troposphere) and $c_{pd} = 1004$ J kg^{-1} K^{-1} is the specific heat capacity of the dry air for constant pressure. This is depicted in Figure 6 for the troposphere and lower stratosphere.

Another limiting case is the moist (pseudo-)isotropic profile, also shown in Figure 6. To calculate it we have used the following equation (Beers, 1945, p. 359; Koutsoyiannis, 2000) which gives a satisfactory approximation for both the isentropic change of saturated air (in which the liquid water remains in the space considered) and saturated pseudo-adiabatic change (in which the liquid water precipitates immediately):

$$c_{pd} \ln T - R_{\mathrm{d}} \ln\big(p - e(T)\big) + \frac{\lambda\, r(T)}{T} = \text{const} \tag{4}$$

In this, $R_{\mathrm{d}} = 287$ J kg^{-1} K^{-1} is the gas constant of dry air, $\lambda = (3.139 \times 10^6 - 2336\, T/\mathrm{K})$ J kg^{-1} is the latent heat of vaporization, and $e(T)$ and $r(T)$ are the saturation water vapor pressure and mixing ratio, respectively, for temperature T. The former is given by the Clausius-Clapeyron equation, as reformulated for water vapor by Koutsoyiannis (2012):

$$e(T) = e_0 \exp\left(24.921\left(1 - \frac{T_0}{T}\right)\right)\left(\frac{T_0}{T}\right)^{5.06}, \qquad T_0 = 273.16 \text{ K}, \qquad e_0 = 6.11657 \text{ hPa} \tag{5}$$

with T_0 and e_0 representing the coordinates of the triple point of water. The mixing ratio is

$$r(T) = \frac{\varepsilon\, e(T)}{p - e(T)} \tag{6}$$

where $\varepsilon = 0.622$ is the ratio of molar masses of water vapor and dry air.

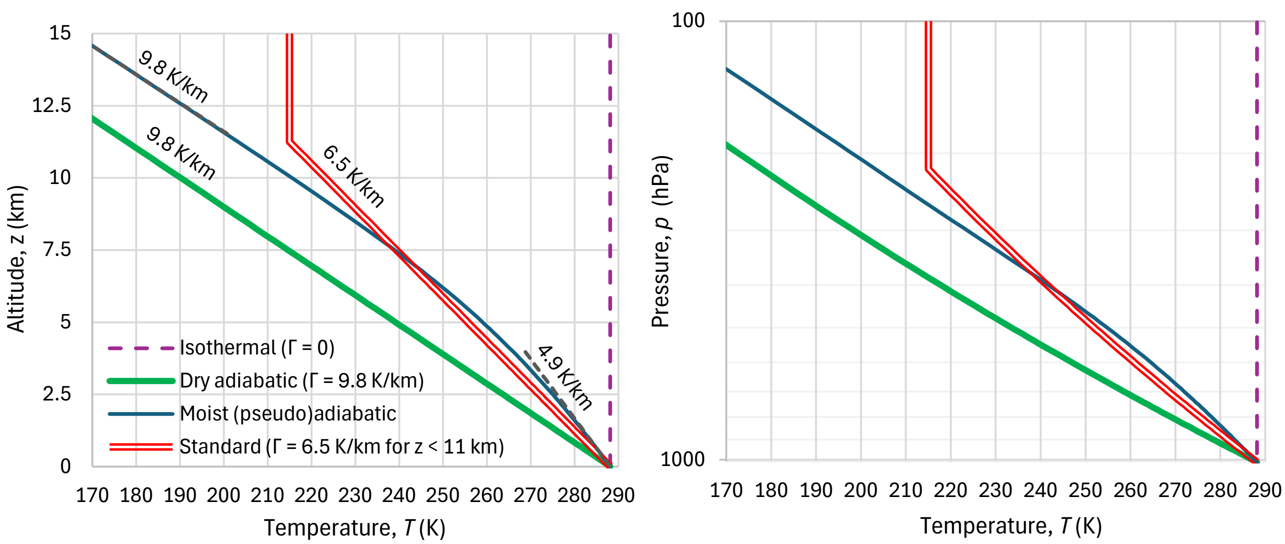

Figure 6 Comparison of different models of temperature profiles of Earth's troposphere, in terms of (**left**) altitude and (**right**) pressure (in logarithmic axis).

It is seen in Figure 6 that the moist adiabatic atmosphere does not have a constant temperature gradient. Rather the gradient is low (4.9 K/km) at the surface and becomes equal to the dry adiabatic rate (9.8 K/km) at high altitudes. The standard atmosphere has a profile close, but not identical, to that of the moist adiabatic one. Its slope is constant (6.5 K/km) for the entire troposphere. The differences become large at high altitudes near the tropopause and above.

It is useful to compare these profiles with observational data. To this aim, we enroll in the ERA5 reanalysis over the period 1940 – 2024 and find the global average temperature over this period at the available pressure levels, as well as the global average geopotential heights for these pressure levels. The results, areally averaged over the torrid and the north frigid zones, are shown in Figure 7. To adapt the standard profile to the conditions of Figure 7 we take the following steps: (a) we replace the standard ground temperature of 288.15 K with the average temperature of the zone at 1000 hPa, (b) We apply the standard gradient $\Gamma = 6.5$ K/km up to the altitude where the temperature takes the standard stratospheric value of 216.65 K, and (c) we keep a constant value of 216.65 K above this altitude up to 20 km.

We observe that in the tropics the actual average temperature profile is located between those of the moist adiabatic and the standard atmosphere, but above 12.5 km it is closer to the former than the latter. However, in the polar area, observations are totally irrelevant to the moist adiabatic profile. Notice that the moist adiabatic conditions would suggest greater gradients in colder conditions (right panel) than in hotter (left panel) because of the Clausius-Clapeyron equation which results in lower WV quantities for lower temperatures (compare the gradients at the surface level, 4.4 and 7.7 K/km in the two panels). The reality is the exact opposite as seen in Figure 7 (see also Figure 12 and Figure 13 below). This means that the moist adiabatic process, despite often being invoked in the literature to explain atmospheric conditions, is not sufficient a tool to describe and explain what happens in reality. All these support the conclusion that the standard atmosphere, despite its empirical basis and its low explanatory power, is more representative for the entire range of conditions on Earth, while the moist adiabatic profile is representative only for the tropics. The dry adiabatic profile is always very different from average conditions. For this reason, the analyses that follow are based on the standard atmosphere.

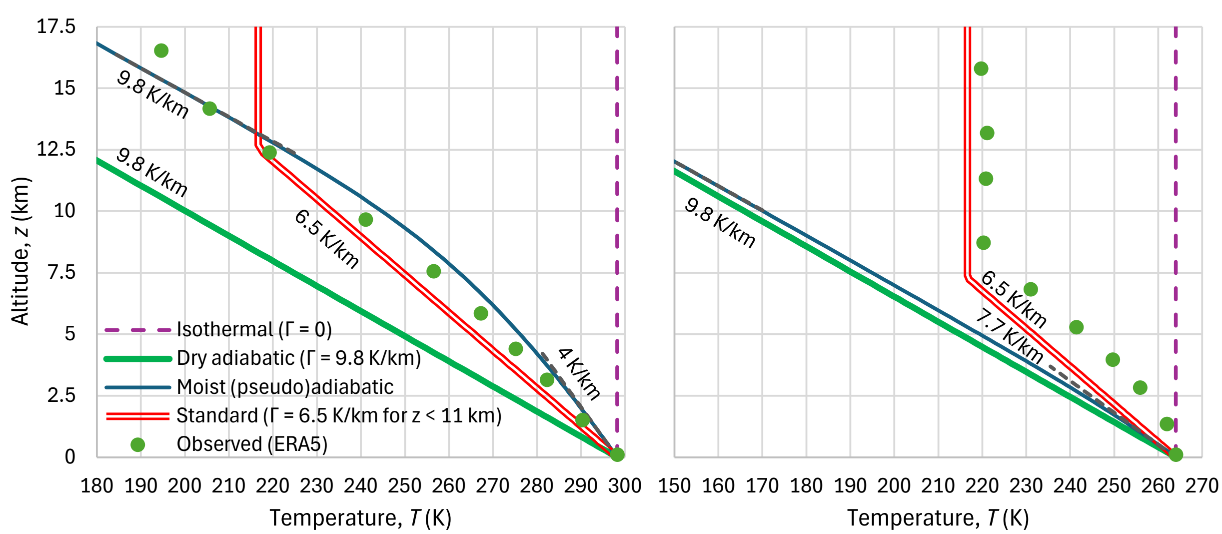

Figure 7 Comparison of temperature profile models of Earth's troposphere with the mean annual observed temperature profile as given by ERA5 reanalysis, temporally averaged over the period 1940 – 2024 and areally averaged over (**left**) the torrid zone and (**right**) the north frigid zone.

3.4 Is the ARE responsible for the observed temperature profile in the atmosphere?

To address the question in the heading, we apply the established greenhouse theory, without considering doubts that have been cast on the validity of the theory or alternative hypotheses (e.g. Nikolov and Zeller, 2017, Miskolczi, 2023). Rather, we enroll the RRTM software, which calculates at each atmospheric level *z* the SW and LW radiation going up and down, namely the four quantities $R_{\mathrm{SW_{up}}}, R_{\mathrm{SW_{down}}}, R_{\mathrm{LW_{up}}}, R_{\mathrm{LW_{down}}}$. While, due to its "rapid" characteristic this software is not the most accurate, we deem it satisfactory for the exploratory character of this research. Taking the differences at two adjacent levels z_1, z_2 we calculate the quantities $\Delta R_{\mathrm{SW_{up}}}, \Delta R_{\mathrm{SW_{down}}}$, $\Delta R_{\mathrm{LW_{up}}}, \Delta R_{\mathrm{LW_{down}}}$, the total radiative energy imbalance ΔR_{tot}, and finally the radiative energy imbalance slope, REIS, based on the following equations.

$$\Delta R_{\mathrm{tot}} \coloneqq \Delta R_{\mathrm{SW_{up}}} + \Delta R_{\mathrm{SW_{down}}} + \Delta R_{\mathrm{LW_{up}}} + \Delta R_{\mathrm{LW_{down}}}, \qquad \mathrm{REIS} \coloneqq \frac{\Delta R_{\mathrm{tot}}}{\Delta z} \tag{7}$$

By convention, *R* quantities directed up are taken as positive and those directed down as negative. If REIS turns out to be positive at a certain layer, between the levels z_1, z_2, this means that the layer receives energy of another type, such as sensible or latent thermal energy. This should be equal to REIS, so that the total energy balance be reinstated.

Figure 8 depicts examples of these quantities between the elevations *z* = 0 and *z* = 426 m (the fourth altitude given as output by RRTM) and for conditions specified in the figure caption, which include both RAGs and clouds. Two cases are examined, an isothermal atmosphere (Γ = 0) and the standard atmosphere (Γ = 6.5 K/km). In the former case, REIS is almost zero, which means that no forcing appears to drive the atmospheric state away of the equilibrium. Therefore, the atmosphere would remain at the equilibrium (isothermal) state, despite the presence of RAGs and clouds.

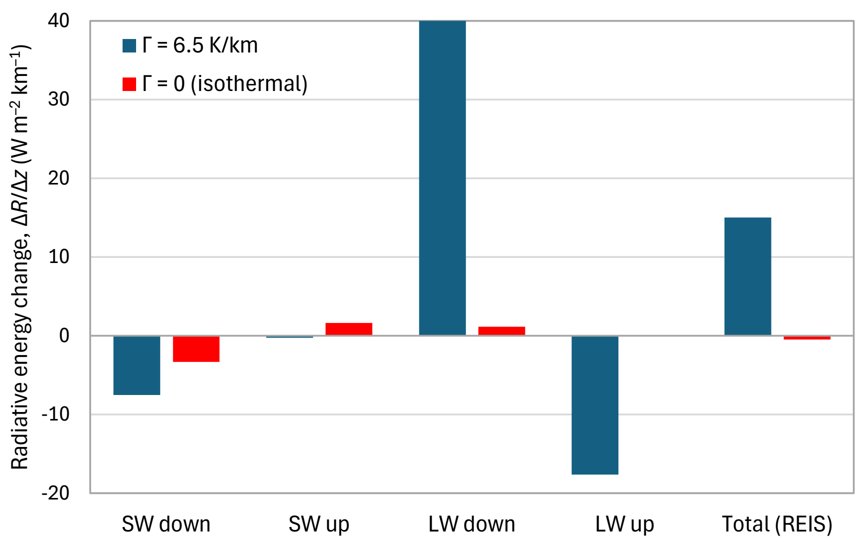

Figure 8 Radiative energy change (SW and LW) between the elevations *z* = 0 and *z* = 426 m and for the indicated cases with default values of RRTM plus clouds, both low and high, each with a fraction of 0.5. For an isothermal atmosphere (Γ = 0) the REIS is almost zero, while for the standard atmosphere gradient (Γ = 6.5 K/km) there is a positive REIS, which means that the total energy balance is reinstated by other energy forms.

In contrast, for the standard atmosphere gradient a positive REIS appears, which means that the total energy balance needs to be reinstated by other energy forms. These forms are indeed present and are the sensible heat due to warm air parcels moving from the Earth's surface up, and the latent heat due to evaporation, again moving from the surface up.

A more complete picture is provided in Figure 9, where REIS is calculated and plotted for the entire range of altitudes modeled by RRTM, for four different cases of ARE (RAG with clouds, RAG without clouds, no NC RAG with clouds, no NC RAG without clouds) and for two cases of temperature gradient, $\Gamma = 6.5$ K/km (standard atmosphere; upper row of panels) and $\Gamma = 0$ (isothermal atmosphere, lower row of panels). What was discussed with respect to Figure 8 is confirmed in Figure 9 for all cases examined and for all altitudes in the troposphere. The isothermal case yields almost zero REIS in the entire troposphere ($z < 11$ km) in all cases, which means that the presence of RAG, whether NC or WV, is not enough for the observed gradient to emerge.

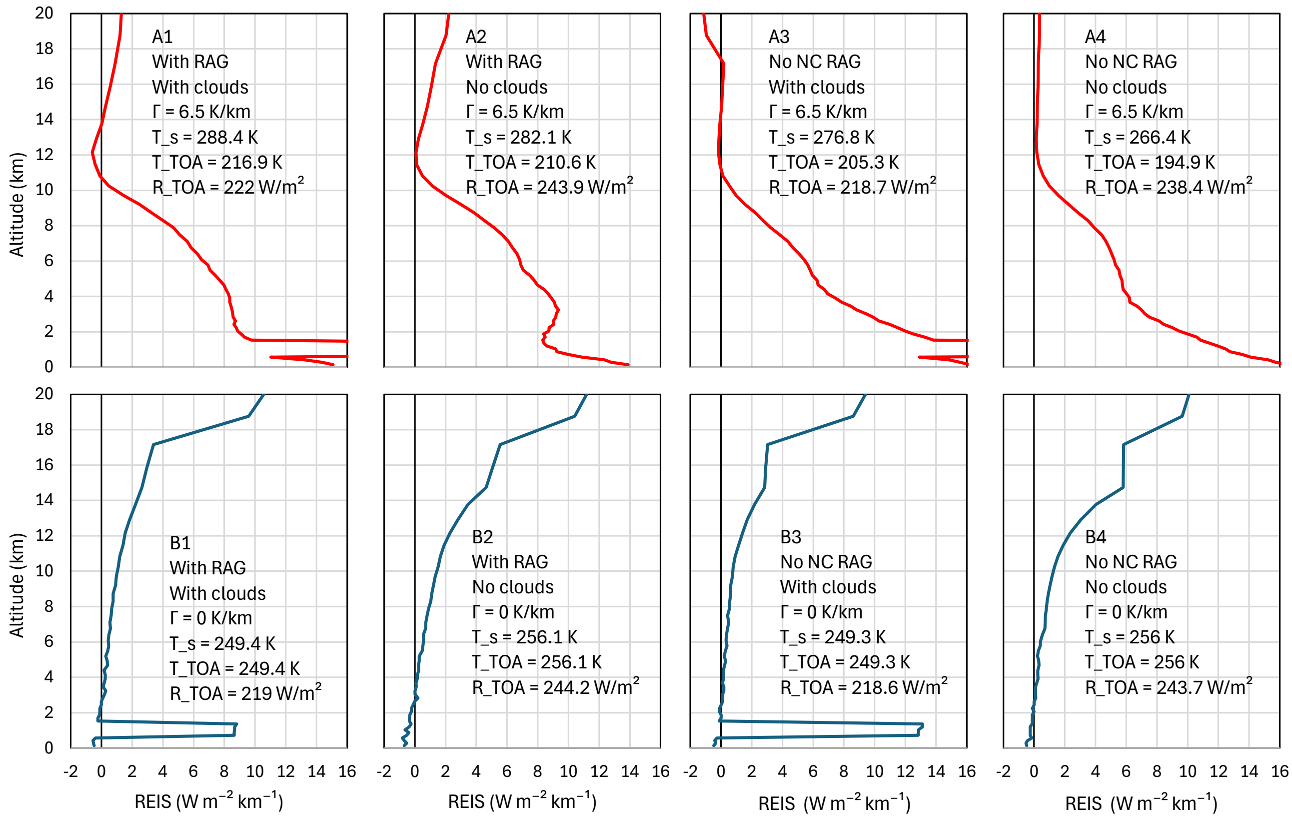

Figure 9 Total (SW and LW) radiative energy imbalance as a function of altitude for the indicated cases. In the upper row the gradient is $\Gamma = 6.5$ K/km, as in the standard atmosphere, while in the lower row there is no gradient (isothermal atmosphere, $\Gamma = 0$). The temperature at the surface (T_s) and the top of atmosphere (T_TOA) are determined by the RRTM so as to equilibrate the incoming net SW (incoming minus outgoing) and the outgoing LW radiation at the top of atmosphere (R_TOA). The default values of RRTM parameters are used wherever it is not noted otherwise. In cases A1, A3, B1 and B3 the clouds referred to are both low and high, each with a fraction of 0.5. The spikes appearing at altitudes around 1 km are due to low clouds. Although in an isothermal atmosphere, clouds would not be formed, for comparison the imaginary cases B1 and B3 assume the existence of clouds, similar to cases A1 and A3.

On the other hand, with the standard atmosphere gradient (Γ = 6.5 K/km) there is a positive REIS in the entire troposphere, which leaves room for sensible and latent heat to act, reinstating the total energy balance and stabilizing the temperature gradient.

3.5 What factors can explain the observed temperature profile?

Given the analysis of the previous subsection, it becomes clear that it is not the ARE that creates and maintains the temperature gradient. Rather the mechanisms responsible for ARE are:

- the warming of the soil and liquid water by the sunshine during the day and their cooling during the night;
- the water evaporation and transpiration at the surface level and condensation aloft;
- the convection, and the implied vertical transfer of sensible and latent heat;
- the winds caused by spatial temperature differences and influenced by Coriolis forces.

These are not static forcings, but processes, i.e. perpetual changes in the climatic system. The processes occur on different time scales, some of which are too small to drive the atmosphere to the equilibrium (isothermal) state. It is noted that the processes occur at a macroscopic level, with the motion of masses of air, typically referred to as parcels. And as noted by van Wijngaarden and Happer (2023), because of the very small thermal conductivity of air, it takes a very long time for appreciable heat to flow into or out of a parcel of reasonable size.

The driving mechanisms of these processes are the following:

1. Clouds form and disappear, strongly affecting the SW and LW radiation processes.
2. The Earth's surface is not homogeneous in terms of SW radiation absorption and reflection (varying albedo).
3. Earth is round (not flat) and the sunrays come with different slopes at different places.
4. Earth rotates around its axis on a daily basis.
5. Earth rotates around the Sun on an annual basis.
6. Earth's orbit around the Sun is elliptical, resulting in changes in the distance between the two bodies.
7. The climatic system is complex and is subject to irregular changes.

A rough quantification of changes produced by these mechanisms is shown in Table 1, where it is seen that some of them are of the order of 100%, reaching the absolute maximum of 200%. This quantification is just indicative and is unable to quantitatively predict the observed temperature profiles as already seen in Figure 7. It is also unable to produce the standard temperature gradient of 6.5 K/km, which here we regard as an empirical model with satisfactory accuracy in representing the average conditions over the entire globe. It incorporates all mechanisms discussed here, but it can hardly be inferred from them by deduction. Sometimes the literature connects it to the moist adiabatic profile but the data above (particularly the right panel in Figure 7) do not support this idea.

Table 1 Typical changes that cause departure from the isothermal atmosphere and their quantified effect on SW radiation processes. R_1 and R_2 denote the downwelling solar radiation at the surface level for the specified conditions 1 and 2, respectively; φ, α and C denote the latitude, albedo and cloudiness, respectively. The calculations are based on Koutsoyiannis (2000) and van Wijngaarden and Happer (2023).

	Reason	Time scale	Assumptions	Condition 1	Condition 2	R_1 (W/m²)	R_2 (W/m²)	% change*
1	Change from clear to cloudy sky	Hours	$\varphi = 45°$, $\alpha = 0.3$, January	Clear sky ($C = 0$)	Cloudy sky ($C = 1$)	74	25	100
2	Spatial change of albedo[§]	Hours	$\varphi = 45°$, $C = 0$, January	Land ($\alpha = 0.3$)	Sea ($\alpha = 0.05$)	74	100	30
3	Change of latitude[§]	Hours	$\alpha = 0.3$, $C = 0$, January	$\varphi = 45°$	$\varphi = 46°$	74	70	5
4	Change from daylight to night	Daily	$\varphi = 45°$, $\alpha = 0.3$, $C = 0$, January	Daylight	Night	197	0	200
5	Change in the angle of incidence of the sun's rays	Annual	$\varphi = 45°$, $\alpha = 0.3$, $C = 0$, January	January	July	74	245	107
6	Changing distance between Earth and Sun	Annual	$\varphi = 0°$, $\alpha = 0.3$, $C = 0$	January	July	220	206	7
7	Recent global warming	Decades	Global average conditions	Before	After	160.6	161	0.2

$*2|R_1 - R_2|/(R_1 + R_2) \times 100$.

[§] Spatial changes are translated into temporal changes assuming wind velocity of 10 m/s.

3.6 What is the relative importance of ARE and temperature gradient in climate dynamics?

The information provided in the different panels of Figure 9 includes the surface temperature at each of the cases examined (A1-A4, B1-B4). A summary of the results is given in Figure 10, along with some additional hypothetical cases. The first imaginary-world case is a planet shaped as a disk perpendicular to the Sun's rays, without an atmosphere and receiving the average radiative energy that the Earth does. In this case, the so-called effective temperature is easy to calculate from the Stefan-Boltzmann law, i.e.,

$$T_0 = \left(\frac{I}{4}\,\frac{1-\alpha}{\varepsilon\sigma}\right)^{\frac{1}{4}} \tag{8}$$

where I = 1360 W/m^2 is the solar irradiance with $I/4$ = 340 W/m^2 representing the average solar energy received by (the spherical) Earth's surface, while σ = 5.67 × 10^{-8} W m^{-2} K^{-4} is the Stefan–Boltzmann constant, ε is the emissivity of the radiating body and α is its albedo. Taking ε = 1 and using the Earth's current albedo $\alpha = 0.3$, so that $(I/4)(1-\alpha) = 238$ W/m^2, the result is $T_0 = 254.5$ K.

About the same (T = 252 K) would be the temperature in the imaginary-world case where there is atmosphere but no ARE (no RAG and no clouds; second bar in Figure 10) or even with NC RAG, but without WV and clouds and without a temperature gradient. If the gradient of 6.5 K/km is present (third bar in Figure 10) the temperature increases to 262 K. Therefore, the effect of the NC RAGs is zero for an isothermal atmosphere and 10 K for an atmosphere with temperature gradient of 6.5 K/km.

In general, in an isothermal atmosphere, the effect of RAGs, including NC RAGs, WV and clouds, is practically zero, as shown by the continuous (blue) line in Figure 10, which fluctuates only slightly, from 249 to 256 K. In contrast, if there is a gradient of 6.5 K/km, the temperature increases up to ~288 K in the realistic case A1, in which the atmosphere contains all RAGs and clouds.

Hence, it is the temperature gradient that makes the surface-level temperature increase from about 252 K (which is close to the average $\overline{T} = 250$ K of Equation (2)) to about 288 K (i.e. by 36 K). This increase is usually attributed to the "greenhouse effect", but it is mainly the result of the temperature gradient, whose origin is not the ARE but the processes described in section 3.5. This is another reason why it is necessary to stop using the term "greenhouse effect" when talking about the climatic system.

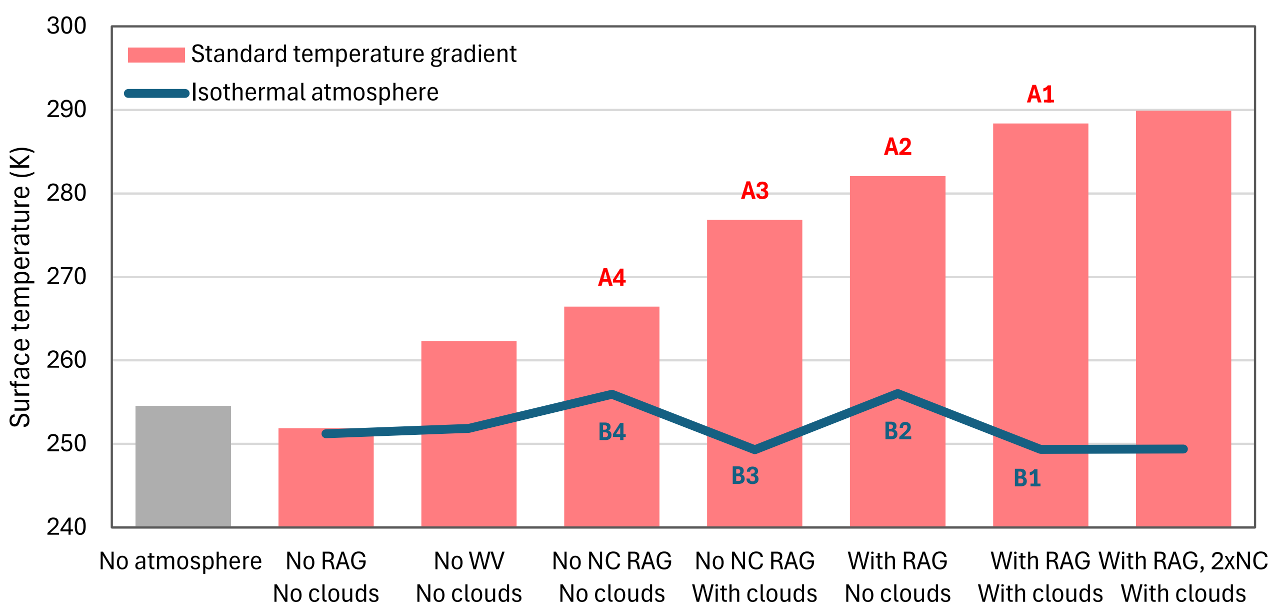

Figure 10 Surface temperature for the cases shown in Figure 9 (A1-A4, B1-B4), in comparison with four additional hypothetical cases: the three cases on the left are for no atmosphere, no RAG at all and no WV (and hence no clouds); the rightmost case is similar to A1/B1 but with doubled NC RAG, resulting in zero change for the isothermal atmosphere (compared to B1) and 1.5 K increase for an atmosphere with standard gradient (compared to A1).

We stress that, among the various cases shown in Figure 10, only cases A1 and A2 are realistic, while all the others are hypothetical. A final hypothetical case shown at the rightmost end of the figure is where the NC RAGs are doubled. This results in a temperature increase of zero in comparison to case B1 or 1.5 K in comparison to case A1. Such an increase ought not to create any concern related to the future of our planet.

While the temperature gradient is the determinant factor that maintains the Earth's temperature much higher than the effective temperature of 254.5 K, with the mechanisms causing this gradient being also causes of maintaining warm conditions, the RAGs also play a significant role as can be inferred from Figure 10. An atmosphere free of RAGs and clouds would keep the temperature close to the average, i.e. 252 K (second bar in Figure 10). Without NC RAGs but with WV and clouds, the surface temperature would be 277 K (case A3)—a substantial increase.

While Figure 10 provides information on the importance of different agents of Earth's warming, it should be stressed that the figure compares the realistic cases (A1, A2) with several imaginary-world cases (all others). Hence, it cannot be a basis for understanding the importance of its factor in real-world conditions. The scientific approach for the latter task is to determine the partial derivatives of a suitable multivariate function representing the ARE, such as the downwelling or outgoing LW radiation, at the point of the current conditions and compare them. Such an analysis has been done in Koutsoyiannis (2024b) with the following resulting percent contributions: (a) for downwelling LW radiation, WV and clouds 95%, CO_2 4%, all other 1%; (b) for outgoing LW radiation, WV and clouds 87%, CO_2 5%, all other 8% (primarily due to the influence of the stratospheric ozone).

Water vapor, besides being the determinant RAG and also the cause of clouds, has another big difference from CO_2: the fact that its quantity in the atmosphere varies substantially over time and space, makes it an agent of perpetual change on all time scales. Relevant changes mostly on hourly to annual time scales have already been described in section 3.5. However, changes also occur at decadal, centennial scales and beyond. These long-term changes are inherent in all geophysical processes, including hydroclimatic ones, and are described in stochastic terms by the so-called Hurst-Kolmogorov dynamics (Koutsoyiannis, 2013, 2021, 2024a; O'Connell et al., 2016; Dimitriadis et al., 2021).

As far as long-term changes are concerned, the CERES satellite data show a decline in the albedo of about 0.004 for the entire observation period (post 2000), which translates to 1.4 W/m^2 (higher than the average imbalance of 0.4 W/m^2 shown in case 7 of Table 1). This has nothing to do with the increase of CO_2 concentration but is consistent with an observed decline in cloud area fraction (Koutsoyiannis et al., 2023, Appendix A.2; Koutsoyiannis and Vournas, 2024, Appendix B; see also Goode et al., 2021; Nikolov and Zeller, 2024). Interestingly, a recent study by Goessling et al. (2025) identifies a record-low planetary albedo in 2023, apparently caused largely by a reduced low-cloud cover in the northern mid-latitudes and tropics, in continuation of a multi-annual trend, all of which contributing to the recent global temperature surge.

Coming back to the results shown in Figure 10, a relevant issue to stress is that the analysis made is unidimensional. Is that representative for the average condition of Earth, which is spherical? A negative reply has been suggested by Nikolov and Zeller (2017), who showed that the mean physical temperature of a spherical body is always lower than its effective radiating temperature computed from the globally integrated absorbed solar flux. This happens because of Hölder's inequality between integrals and the fact that Stefan-Boltzmann law is a power law with an exponent 4.

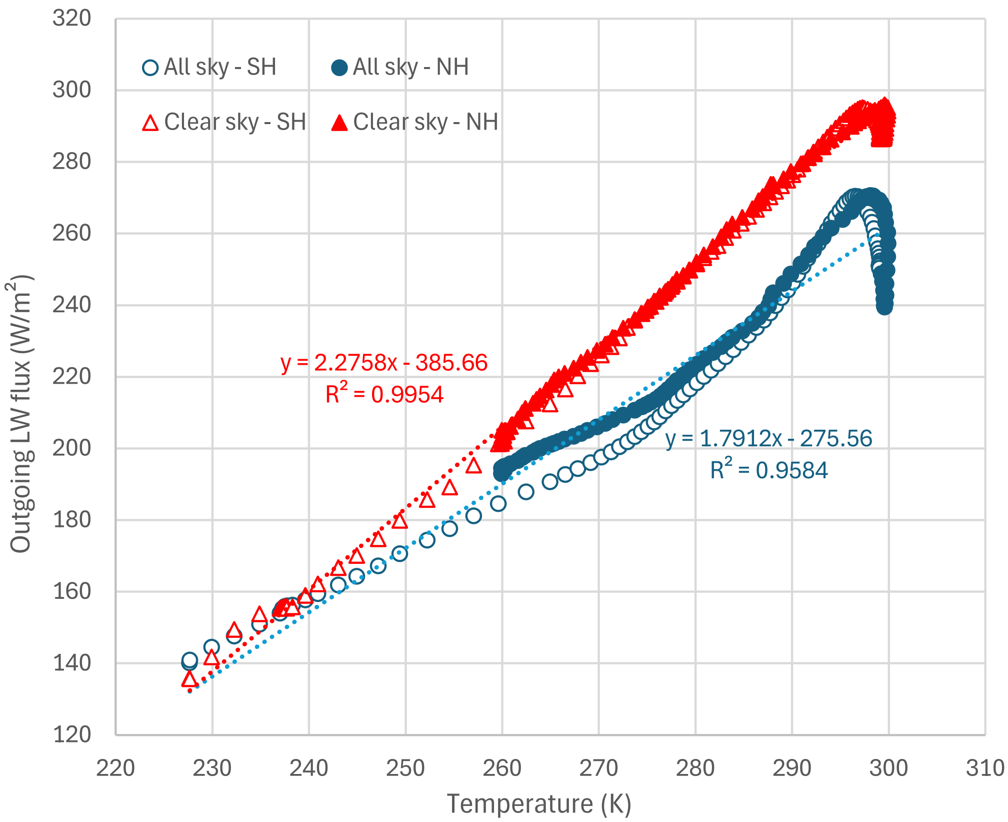

Figure 11 Outgoing LW radiation vs. ground temperature. Each point refers to the zonal average of LW radiation (for clear sky and all sky) averaged from 2000 to 2022 as given by the CERES data and the zonal average of ground temperature as given by ERA5 Reanalysis; the resolution is 1° (180 points in total). Temperature data from ERA5 Reanalysis retrieved from the Climexp platform; radiation data retrieved from https://ceres-tool.larc.nasa.gov/ordtool/jsp/SSF1degEd41Selection.jsp.

This suggestion indeed makes sense for the condition of a planet without an atmosphere (first bar in Figure 10), where an integration over the Earth's sphere would result in a lower value than shown in the figure. However, if we consider the realistic conditions of Earth, in particular cases A1 and A2 of Figure 10, rather than the imaginary-world conditions, the cautionary note by Nikolov and Zeller does not apply. For the relationship between outgoing radiation and temperature is no longer a power law but a virtually linear relationship, as shown in Figure 11, constructed from CERES radiation data and ERA5 Reanalysis near-surface temperature data. Additional information on this linear relationship is provided by Koll and Cronin (2018, Fig. 1) and Koutsoyiannis (2024b, Fig. 6), which in essence confirm early observations and analyses by Budyko (1969). Hence, the quantities depicted in Figure 10 are representative of average conditions for the (spherical) Earth, at least for the realistic cases A1 and A2, albeit not for the imaginary case of an atmosphere-free Earth.

3.7 What are the recent changes in the atmospheric temperature gradient?

Once we have recognized the temperature gradient as a critical factor determining the climate, it is useful to monitor and analyze its changes, which are certainly much more influential than the famed changes in CO_2 concentration. To this end, Figure 12 (upper) shows the variation of the atmospheric temperature averaged over the five geographical zones at two pressure levels, 1000 and 200 hPa, as given by the ERA5 reanalysis. By using the geopotential height at these pressure levels, also available in the ERA5 dataset, we determined and plotted in Figure 12 (lower) the evolution of the temperature gradient per geographical zone, calculated as the (minus) ratio of differences of temperature and geopotential heights between these two levels.

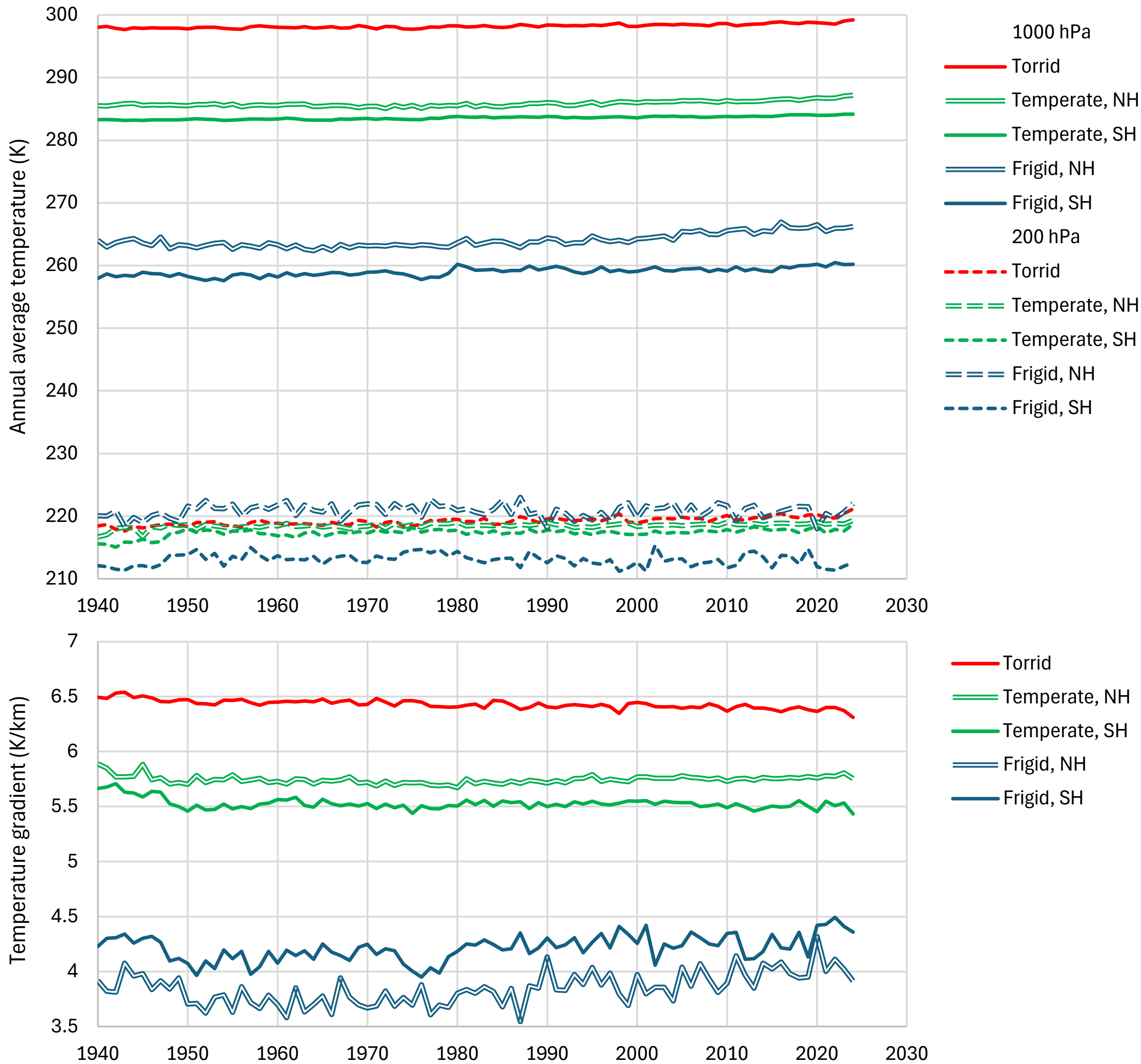

Figure 12 (**upper**) Evolution of mean annual air temperature averaged over the five geographical zones at the levels of 1000 and 200 hPa. (**lower**) Evolution of the temperature gradient per geographical zone, calculated as the (minus) ratio of differences of temperature and geopotential heights between these two levels. Data from ERA5 Reanalysis retrieved through NOAA's WRIT.

It is clear from Figure 12 that, as we move from the equator to the poles and the surface temperatures decrease, so do the temperature gradients. This is fully compatible with the analyses of section 3.4-3.6, according to which higher gradients lead to higher surface temperatures (see also Figure 13, left).

Surface temperatures present increasing trends over time in all zones. In contrast, the temperatures at the level of 200 do not show geographical or temporal changes. It is interesting to examine the temporal trends of temperature gradients, visualized in Figure 12 (lower) and summarized in Figure

13 (right). At the torrid zone we observe a falling trend, which can be viewed as negative feedback to the increasing surface temperatures. In contrast, at the frigid zones the trends are increasing, and hence we would expect greater warming. In the temperate zones no notable trends appear.

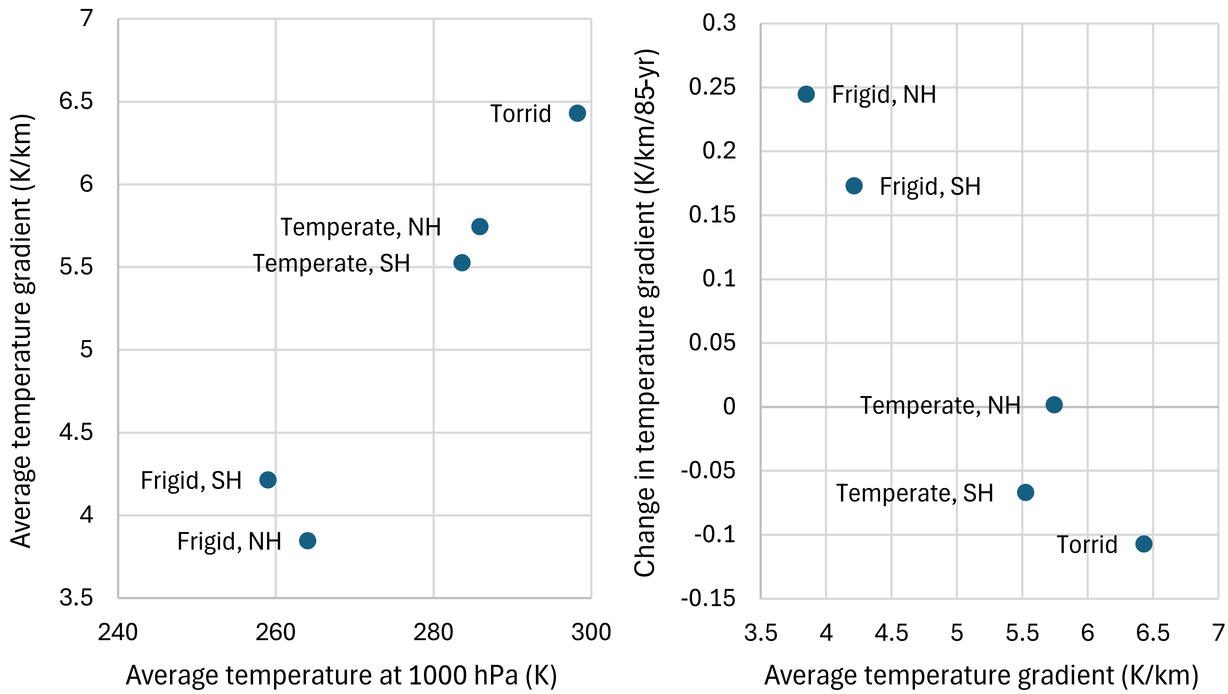

Figure 13 (**left**) Average temperature gradient per geographical zone (calculated as indicated in the caption of Figure 12) vs. average temperature. (**right**) Change in temperature gradient per geographical zone over the 85-year period of ERA5 data availability (calculated from the slope of linear trends fitted to the curves of Figure 12, lower).

Indeed, the zonal distribution of the climatic surface temperature differences between the latest and oldest 30-year periods (for which ERA5 Reanalysis data are available in the CLIMEXP platform), seen in Figure 14, confirm these observations. The figure plots show that for the greatest part of Earth, between latitudes 50°S and 50°N there has been a warming trend of about 1.4 K/century, slightly increasing as we move north, as the percentage of land increases. Between 50°N and the Arctic Circle there is a further warming trend, while between 50°S and the Antarctic Circle the trend becomes cooling. The greatest increases of surface temperature are observed in the frigid zones, where we have increasing temperature gradient trends.

All the above observations are consistent with the evidence from paleoclimatic studies, which suggests that the surface equator-to-pole temperature gradients were weaker during warm periods, while tropical temperatures changed very little (Budyko, 1977, p. 17; Huber et al., 2000, p. 289; Huber, 2008; Lee, 2014; Lindzen, 2020). They are also consistent with the recent study by Ma et al. (2025), which identified wind stilling (compatible with the decrease in the surface equator-to-pole temperature gradient), which resulted in weakened evaporation in two-thirds of the ocean and a slight decreasing trend in global-averaged ocean evaporation during 2008–2017. According to the established climate narrative, the temperature rise should have increased evaporation, not decreased it. Such paradoxes would have been avoided if the climate alterations were not attributed to a single cause, the burning of fossil fuels and the "chain reaction" it allegedly triggers.

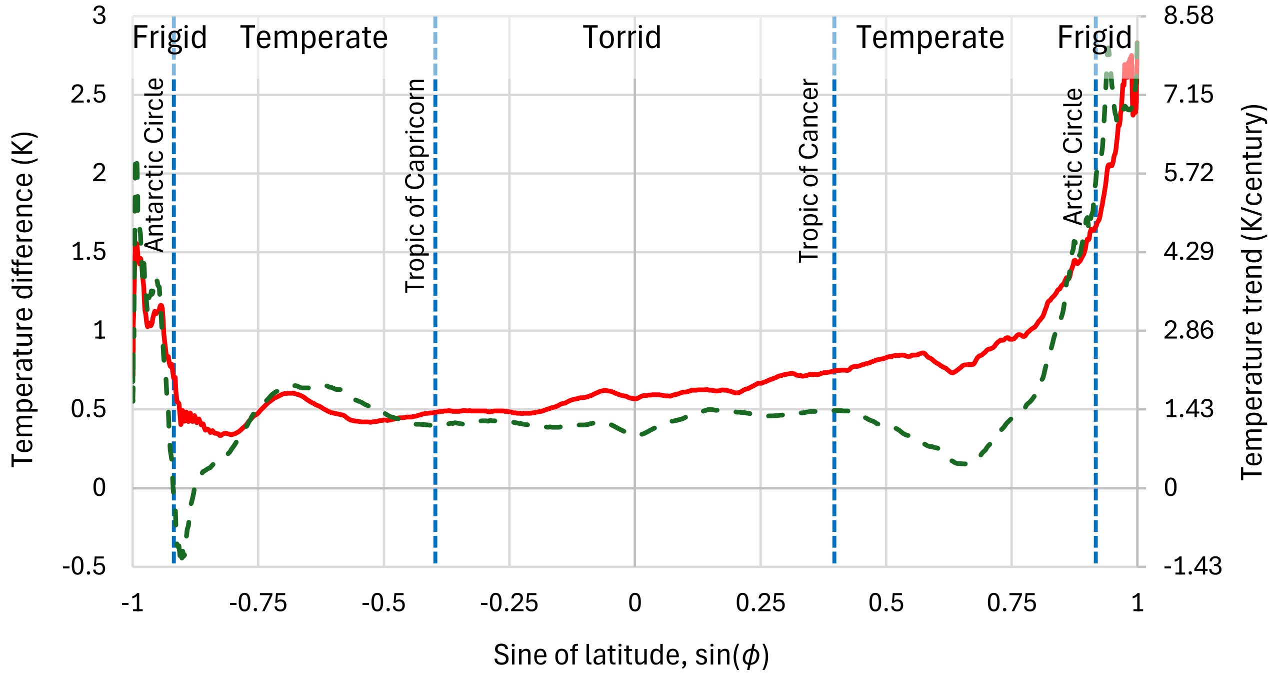

Figure 14 Difference of average surface temperatures, as a function of the sine of latitude, of two 30-year climatic periods, namely of the most recent 1995 – 2024 minus the 1950 – 1979. Continuous line represents the average over the globe, while dashed line represents the average over the area between longitudes 155°E and 130°W, mostly covered by sea (Pacific, Arctic and Southern Oceans). The sine of latitude was chosen as the horizontal axis so that increments be proportional to the respective areas on Earth. Data from ERA5 reanalysis; data retrieval and processing from the Climexp platform (processing steps: (a) subsetting for each of the two periods; (b) aggregation to annual (Jan-Dec) time resolution; (c) compute zonal mean; (d) compute mean, s.d. [standard deviation], or extremes).

4 Discussion and conclusions

The political origin of the climate agenda has contaminated the scientific vocabulary with popular slogans that are not appropriate scientific terms, including “greenhouse effect” and “settled science”, which are examined in this paper, as well as many more (“climate crisis”, “climate emergency”, “climate destabilization”, “climate destruction”, “climate catastrophe”, “climate apocalypse”, “climate existential threat”, “global boiling”, “global burning”, all of which expressions are found in papers indexed in Google Scholar as the reader can readily verify).

The research presented here shows that we do not live in a greenhouse and that science cannot be settled. Rather, it is useful to revisit even the most fundamental topics related to climate. This has been attempted in this study in the simplest possible way and using the fewest premises, such as Newton’s laws, the principle of maximum entropy and the spectroscopic properties of gases. Additionally, non-scientific jargon has been replaced by scientific terminology, the main examples being that “greenhouse gas” has been replaced by “radiatively active gas” (RAG, comprising water vapor—WV—and non-condensing radiatively active gases—NC RAG) and the term “greenhouse effect” with “atmospheric radiative effect” (ARE).

The conclusions of the analyses presented here can be summarized as follows:

- There is an empirically verified ARE in the atmosphere, not only on Earth but also on the other planets. On Earth, ARE is dominated by WV and clouds, with CO_2 playing a very minor role—let alone human added CO_2 which represents only 4% of the total emissions to the atmosphere.
- Equilibrium thermodynamics clearly show (either using the principle of maximum entropy, or stochastic simulation of molecule collisions) that Earth's atmosphere would be isothermal at the equilibrium, with or without RAGs. In an isothermal atmosphere the temperature would be slightly higher than 250 K, a value which represents the vertically average temperature of the standard atmosphere over the troposphere and stratosphere.
- The fact is that the atmosphere is not isothermal. Rather, the troposphere has a vertical temperature gradient of about 6.5 K/km, which is imprinted in the standard atmosphere. The gradient is resultant of macroscopic changes that drive the atmosphere out of equilibrium. While the moist adiabatic changes play a role in shaping this gradient, they cannot fully predict real atmospheric conditions.
- The mean surface temperature of 288 K, also imprinted in the standard atmosphere, is much higher than the equilibrium temperature. While ARE plays a role in yielding this temperature (mostly WV and clouds), the critical factor is the vertical temperature gradient, without which the ARE alone would not be able to increase the equilibrium temperature.
- Given the importance of the atmospheric temperature gradient, along with the fact that it is not a universal constant since it varies with space and time, it is useful to monitor and analyze its changes. The data show that since 1950 the gradient has weakened in the tropics and grown in the polar areas resulting in decrease of the surface equator-to-pole gradient, as expected in global warming conditions.

A final reminder worth stressing is that in complex systems, such as the climatic system, observational data are the only scientific test bed for making hypotheses and assessing their validity. The real-world data do not agree with the mainstream "climate science" (a euphemism for sophistry).

Appendix A: Maximum entropy of a single monoatomic molecule

We consider an air column with a square cross section of edge a containing monoatomic molecules of mass m_0, assumed to be spherical particles, in fast motion. We do not know their exact position and velocity (actually, it is infeasible to know them). We wish to find the marginal probability distribution of one of these particles. Its state is described by 6 variables, 3 indicating its position $\underline{x}_i$ and 3 indicating its velocity $\underline{u}_i$ with $i = 1,2,3$, all represented as stochastic variables, forming the vector $\underline{\boldsymbol{z}} = \left(\underline{x}_1, \underline{x}_2, \underline{x}_3, \underline{u}_1, \underline{u}_2, \underline{u}_3\right)$. Notice that here we use the Duch convention to underline stochastic (random) variables, while their values are not underlined. We denote $f(\boldsymbol{z})$ the probability density function. The constraints for the particle's position are:

$$0 \le \underline{x}_{1,2} \le a, \qquad x_3 \ge 0 \tag{A1}$$

We use a non-relativistic framework and therefore we do not constrain velocity. The feasible space, Ω, is thus $\Omega \coloneqq \{0 \le x_{1,2} \le a, x_3 \ge 0, -\infty < u_i < \infty; i = 1,2,3\}$.

As the column is not in motion, conservation of momentum demands that $\mathrm{E}\left[m_0 \underline{u}_i\right] = m_0 \int_\Omega u_i f(\boldsymbol{z}) \mathrm{d}\boldsymbol{z} = 0$, or:

$$\mathrm{E}\left[\underline{u}_i\right] = 0, \qquad i = 1,2,3 \tag{A2}$$

We note that, in general, the expectation $\mathrm{E}\left[\underline{u}_i\right]$ represents macroscopic motion, while $u_i - \mathrm{E}\left[\underline{u}_i\right]$ represents fluctuation at a microscopic level. (In our case the fluctuation is identical to u_i.)

The conservation of energy demands that the sum of *internal* (or *thermal*) *energy* and the dynamic energy of the particle be constant, equal to the energy per particle, ε. The former is $\mathrm{E}\left[m_0\left\|\underline{u}\right\|^2/2\right] = (m_0/2)\int_\Omega \left\|\underline{u}\right\|^2 f(\boldsymbol{z})\mathrm{d}\boldsymbol{z}$, where $\left\|\underline{u}\right\|^2 = \underline{u}_1^2 + \underline{u}_2^2 + \underline{u}_3^2$, and the latter is $m_0 g \underline{x}_3$, where g is the gravity acceleration. Hence, the energy constraint is

$$\mathrm{E}\left[\left\|\underline{u}\right\|^2 + 2g\underline{x}_3\right] = \frac{2\varepsilon}{m_0} \tag{A3}$$

Now we form the entropy of $\underline{\boldsymbol{z}}$ according to the entropy definition:

$$\Phi\left[\underline{\boldsymbol{z}}\right] \coloneqq \mathrm{E}\left[-\ln\frac{f\left(\underline{\boldsymbol{z}}\right)}{\beta\left(\underline{\boldsymbol{z}}\right)}\right] = -\int_\Omega \ln\frac{f(\boldsymbol{z})}{\beta(\boldsymbol{z})} f(\boldsymbol{z})\mathrm{d}\boldsymbol{z} \tag{A4}$$

where $\beta(\boldsymbol{z})$ is a background density, assumed to be of Lebesgue form. We recognize from the quantity $\ln(f(\boldsymbol{z})/\beta(\boldsymbol{z}))$ that the latter should have units $[\boldsymbol{z}^{-1}] = [x^{-3}]\,[u^{-3}] = [\mathrm{L}^{-6}\,\mathrm{T}^{3}]$. To form this, we utilize a universal constant, i.e., the Planck constant $h = 6.626 \times 10^{-34}$ J s; its dimensions are $[\mathrm{L}^2\,\mathrm{M}\,\mathrm{T}^{-1}]$. If we combine it with the particle mass m_0, we observe that the quantity $(m_0/h)^3$ has the required dimensions $[\mathrm{L}^{-6}\,\mathrm{T}^{3}]$, thereby giving the entropy as

$$\Phi\left[\underline{\boldsymbol{z}}\right] \coloneqq \mathrm{E}\left[-\ln\left(\left(\frac{h}{m_0}\right)^3 f\left(\underline{\boldsymbol{z}}\right)\right)\right] = -\int_\Omega \ln\left(\left(\frac{h}{m_0}\right)^3 f(\boldsymbol{z})\right) f(\boldsymbol{z})\mathrm{d}\boldsymbol{z} \tag{A5}$$

Notice that here we have not multiplied the entropy with the Boltzmann constant $k = 1.381\times10^{-23}$ J K^{-1} and that $\Phi\left[\underline{\boldsymbol{z}}\right]$ is dimensionless.

To apply the principle of maximum entropy with constraints (A1), (A2) and (A3), plus the unity integral of the density function, we form the Lagrangian (using Lagrange multipliers $l_i, i = 0, \dots, 4$):

$$\begin{aligned} A \coloneqq &-\int_\Omega \ln\left(\left(\frac{h}{m_0}\right)^3 f(\boldsymbol{z})\right) f(\boldsymbol{z})\mathrm{d}\boldsymbol{z} - l_0\left(\int_\Omega f(\boldsymbol{z})\mathrm{d}\boldsymbol{z} - 1\right) - \sum_{i=1}^{3} l_i \int_\Omega u_i f(\boldsymbol{z})\mathrm{d}\boldsymbol{z} \\ &- l_4\left(\int_\Omega \left(u_1^2 + u_2^2 + u_3^2 + 2g\underline{x}_3\right) f(\boldsymbol{z})\mathrm{d}\boldsymbol{z} - \frac{2\varepsilon}{m_0}\right) \end{aligned} \tag{A6}$$

Taking the functional derivative, we find

$$\frac{\partial A}{\partial f(\boldsymbol{z})} = -\ln\left(\left(\frac{h}{m_0}\right)^3 f(\boldsymbol{z})\right) - 1 - l_0 - \sum_{i=1}^{3} l_i\, u_i - l_4\left(u_1^2 + u_2^2 + u_3^2 + 2g\underline{x}_3\right) = 0 \qquad \text{(A7)}$$

After algebraic manipulations, we eventually find the distribution of $\underline{\boldsymbol{z}}$ as:

$$f(\boldsymbol{z}) = \frac{2}{\pi^{3/2}}\left(\frac{1}{a}\right)^2 \left(\frac{5m_0}{4\varepsilon}\right)^{5/2} g \exp\left(-\frac{5m_0}{4\varepsilon}\left(\|\underline{u}\|^2 + 2gx_3\right)\right) \qquad \text{(A8)}$$

Indeed, $f(\boldsymbol{z})$ in (A8) satisfies all constraints, as it is trivial to show that:

$$\int_\Omega f(\boldsymbol{z})\,\mathrm{d}\boldsymbol{z} = 1, \qquad \int_\Omega u_i f(\boldsymbol{z})\,\mathrm{d}\boldsymbol{z} = 0, \qquad \int_\Omega (u_1^2 + u_2^2 + u_3^2 + 2gx_3)\, f(\boldsymbol{z})\mathrm{d}\boldsymbol{z} = \frac{2\varepsilon}{m_0} \qquad \text{(A9)}$$

To find the marginal distribution of each of the variables we integrate over the domain of the remaining variables. Thus, the marginal distribution of each of the location coordinates $\underline{x}_i$ is easily found to be,

$$f_{x_1}(x_1) = f_{x_2}(x_2) = \frac{1}{a}, \qquad 0 \le x_1, x_2 \le a, \qquad f_{x_3}(x_3) = \frac{5gm_0}{2\varepsilon}\exp\left(-\frac{5gm_0}{2\varepsilon}x_3\right) \qquad \text{(A10)}$$

As $f_{x_3}(x_3)$ is proportional to air density, the last equation shows that the density decreases exponentially with altitude. The marginal distribution of each of the velocity coordinates $\underline{u}_i$ is derived from equation (A8) as

$$f_{u_i}(u_i) = \left(\frac{5m_0}{4\pi\varepsilon}\right)^{1/2} \exp\left(-\frac{5m_0}{4\varepsilon}u_i^2\right) \qquad \text{(A11)}$$

This is Gaussian with mean 0 and variance $2\varepsilon/5m_0$.

Furthermore, we readily deduce from the above results that the joint distribution $f(\boldsymbol{z})$ is a product of functions of $\boldsymbol{z}$'s coordinates $(x_1, x_2, x_3, u_1, u_2, u_3)$. This means that all six stochastic variables are jointly independent. The independence results from entropy maximization. From (A8) and (A11) we also observe a symmetry with respect to the three velocity coordinates, resulting in equipartition of the total energy ε into $\varepsilon/5$ for each direction or degree of freedom. This is known as the *equipartition* principle and is again a result of entropy maximization. In other words, neither independence nor equipartition are posed as assumptions here. Clearly, they are derived by the principle of maximum entropy (that is, maximum uncertainty).

To find the marginal distribution of the velocity magnitude $\|\underline{u}\|$, we recall that the sum of squares of n independent $N(0,1)$ stochastic variables has a $\chi^2(n)$ distribution (Papoulis, 1990, pp. 219, 221) and then we use known results for the density of a transformation of a stochastic variable (Papoulis, 1990, p. 118) to obtain the distribution of the square root. The result is the Maxwell–Boltzmann distribution:

$$f_{\|\underline{u}\|}(\|\underline{u}\|) = \frac{4}{\sqrt{\pi}}\left(\frac{5m_0}{4\varepsilon}\right)^{3/2} \|\underline{u}\|^2 \exp\left(-\frac{5m_0}{4\varepsilon}\|\underline{u}\|^2\right) \tag{A12}$$

Once $f(\boldsymbol{z})$ has been determined in equation (A8), the mean energy can be partitioned into thermal and dynamic (due to gravity) as follows:

$$\varepsilon_\theta \coloneqq \mathrm{E}\left[m_0\|\underline{u}\|^2/2\right] = \frac{3\varepsilon}{5}, \qquad \varepsilon_g \coloneqq \mathrm{E}\left[m_0 g \underline{x}_3\right] = \frac{2\varepsilon}{5} \tag{A13}$$

Given that the kinetic state of a monoatomic molecule has three degrees of freedom (one per direction of motion), the above result shows that gravity is equivalent to two additional degrees of freedom.

The final expression of entropy is then obtained as follows. We observe that

$$\begin{gathered} -\ln f(\boldsymbol{z}) = 2\ln a + \frac{5}{2}\ln\left(\frac{4\pi\varepsilon}{5m_0}\right) - \ln(2\pi g) + \frac{5m_0}{4\varepsilon}\left(u_1^2 + u_2^2 + u_3^2 + 2gx_3\right), \\ \ln\beta(\boldsymbol{z}) = 3\ln\frac{m_0}{h} \end{gathered} \tag{A14}$$

After performing the integration over Ω we find

$$\Phi[\underline{\boldsymbol{z}}] = \frac{5}{2}\ln\left(\frac{2^{8/5}\pi^{3/5}\mathrm{e}}{5}\,\frac{m_0^{1/5}}{g^{2/5}h^{6/5}}\,\varepsilon a^{4/5}\right) \tag{A15}$$

where e is the base of natural logarithms. It can be verified that the equation is dimensionally consistent and that $\Phi[\underline{\boldsymbol{z}}]$ is dimensionless as it should be.

The temperature is defined as the inverse of the partial derivative of entropy with respect to thermal energy, i.e.,

$$\frac{1}{\theta} \coloneqq \left(\frac{\partial\Phi}{\partial\varepsilon_\theta}\right)_{V,N} \tag{A16}$$

where the meaning of the subscripts is that the volume V and number of particles N should be constant. Notice that in this definition, temperature has units of energy and to convert it to the thermodynamic temperature T we must divide it by Boltzmann constant ($T = \theta/k$). In our case $N = 1$ and the V of the column is infinite, and thus we replace it with the mean of the volume, regarded as a stochastic variable, i.e.

$$\mu_V \coloneqq \mathrm{E}[\underline{V}] = a^2\mathrm{E}[\underline{x}_3] = a^2\int_0^\infty \frac{5gm_0}{2\varepsilon}\exp\left(-\frac{5gm_0}{2\varepsilon}x_3\right)\mathrm{d}x_3 = \frac{2\varepsilon a^2}{5gm_0} \tag{A17}$$

so that, to have constant μ_V the size a should be

$$a = \left(\frac{5gm_0}{2\varepsilon}\mu_V\right)^{1/2} \tag{A18}$$

Equation (A15) can then be written as

$$\Phi[\underline{z}] = \frac{5}{2}\ln\left(\frac{2^{6/5}\pi^{3/5}\mathrm{e}}{3^{3/5}}\,\frac{m_0^{3/5}}{h^{6/5}}\,\varepsilon_\theta^{3/5}\mu_V^{2/5}\right) \tag{A19}$$

Taking the derivative with respect to ε_θ, we easily find

$$\frac{1}{\theta} = \frac{\partial\Phi}{\partial\varepsilon_\theta} = \frac{3}{2\varepsilon_\theta} \Rightarrow \theta = \frac{2\varepsilon_\theta}{3} \tag{A20}$$

The above analysis was made for the entire air column. Next, we will fix the altitude to a specific value x_3 and find the same quantities conditional on this altitude. Using the subscript C for conditional, in this case we have

$$f_\mathrm{C}(\boldsymbol{z}|x_3) = \frac{f(\boldsymbol{z})}{f_{x_3}(x_3)} = \left(\frac{1}{a}\right)^2\left(\frac{5m_0}{4\pi\varepsilon}\right)^{3/2}\exp\left(-\frac{5m_0}{4\varepsilon}\left(\left\|\underline{u}\right\|^2\right)\right) \tag{A21}$$

where we observe that the conditional probability density does not depend on the altitude x_3. Now the integration volume is $\Omega_\mathrm{C} \coloneqq \{0 \le x_{1,2} \le a, -\infty < u_i < \infty; i = 1,2,3\}$. Integrated over this volume, the mean energy is:

$$\varepsilon_\theta = \mathrm{E}\left[m_0\left\|\underline{u}\right\|^2/2\right] = \int_{\Omega_\mathrm{C}}(u_1^2 + u_2^2 + u_3^2)\,f_\mathrm{C}(\boldsymbol{z})\mathrm{d}\boldsymbol{z} = \frac{3\varepsilon}{5} \tag{A22}$$

This is the same as in the unconditional case. The potential energy is fixed, $\varepsilon_g = m_0 g x_3$, and its average over the column is

$$\varepsilon_g \coloneqq \int_0^\infty m_0 g x_3 f_{x_3}(x_3)\mathrm{d}x_3 = \frac{2\varepsilon}{5} \tag{A23}$$

which agrees with the previous result.

The entropy is not easy to calculate in conditional mode, as an assumption is needed for adapting the background measure $\beta(\boldsymbol{z})$. For this reason, we follow a different approach, replacing the condition $\underline{x}_3 = x_3$ with $x_3 - a/2 \le \underline{x}_3 \le x_3 + a/2$, so that no change to the background measure be necessary. In order for this approximation to be valid, we assume $a \ll x_3$, which is not a problem as we can make a as small as we wish. In this case, a uniform distribution for the location of the molecule in the cube is plausible. Based on the results in Koutsoyiannis (2014) and substituting $3\varepsilon/5$ for ε, we have

$$f_{\mathrm{F}}(\boldsymbol{z}) = \left(\frac{1}{a}\right)^3 \left(\frac{5m_0}{4\pi\varepsilon}\right)^{3/2} \exp\left(-\frac{5m_0}{4\varepsilon}\left(\|\underline{u}\|^2\right)\right) \tag{A24}$$

where the subscript F stands for "fixed x_3" and the only difference from Equation (A21) is that a is cubed, rather than squared. The thermal energy is then found to be

$$\varepsilon_\theta = \frac{3\varepsilon}{5} \tag{A25}$$

i.e., the same as above. The entropy is

$$\Phi_{\mathrm{F}}[\underline{\boldsymbol{z}}] = \frac{3}{2}\ln\left(\frac{4\pi\mathrm{e}}{5}\,\frac{m_0}{h^2}\,\varepsilon a^2\right) \tag{A26}$$

and the temperature

$$\frac{1}{\theta_{\mathrm{F}}} = \frac{\partial\Phi_{\mathrm{F}}}{\partial\varepsilon} \Big/ \frac{\partial\varepsilon_\theta}{\partial\varepsilon} = \frac{3}{2\varepsilon}\Big/\frac{3}{5} \Rightarrow \theta_F = \frac{2\varepsilon}{5} = \frac{2\varepsilon_\theta}{3} \tag{A27}$$

which is constant, independent of x_3.

Appendix B: Maximum entropy of a single diatomic molecule

In diatomic gases, which constitute the vast majority in the atmosphere (N_2, O_2), in addition to the kinetic energy, we have rotational energy at two axes x_4 and x_5 perpendicular to the axis defined by the two molecules. These energies are $L_4^2/2I$ and $L_5^2/2I$, where L denotes angular momentum at the two axes x_4 and x_5 (dimensions [M L^2 T^{-1}]) and I denotes rotational inertia (dimensions [M L^2]). due to symmetry, $I_4 = I_5 = I$.

We consider again the same column with square cross section of edge a, containing identical diatomic molecules, each one with mass m_0, rotational inertia I, and sum of kinetic, rotational and dynamic energy ε. Each molecule is described by eight variables, three indicating its position, $\underline{x}_i$, three indicating its velocity $\underline{u}_i$ $(i = 1,2,3)$ and two indicating its rotation, $\underline{u}_4 = \underline{L}_4/\sqrt{Im_0}$ and $\underline{u}_5 = \underline{L}_5/\sqrt{Im_0}$. Note that the coordinates $\underline{u}_4$ and $\underline{u}_5$ were chosen so as have the same dimensions as all other $\underline{u}_i$ and $m_0 u_i^2/2$, $i = 4,5$ represent the rotational energy. The coordinates $\underline{x}_1, \underline{x}_2, \underline{x}_3$ and the five $\underline{u}_i$ are represented as stochastic variables, forming the vector $\underline{\boldsymbol{z}} = (\underline{x}_1, \underline{x}_2, \underline{x}_3, \underline{u}_1, \underline{u}_2, \underline{u}_3, \underline{u}_4, \underline{u}_5)$.

The constraints are the same as in Appendix A ((A1)– (A3)). The background density $\beta(x)$ in $\ln(f(x)/\beta(x))$ should have units [$\boldsymbol{z}^{-1}$] = [x^{-3}] [u^{-5}] = [L^{-8} T^5]. Combining the Planck constant h with the particle mass m_0 and rotational inertia I, we observe that the required dimensions are attained by the quantity $m_0^4 I/h^5$, thereby giving the entropy as

$$\Phi[\underline{\boldsymbol{z}}] \coloneqq \mathrm{E}\left[-\ln\left(\frac{h^5}{m_0^4 I} f(\underline{\boldsymbol{z}})\right)\right] = -\int_{\Omega} \ln\left(\frac{h^5}{m_0^4 I} f(\boldsymbol{z})\right) f(\boldsymbol{z}) \mathrm{d}\boldsymbol{z} \tag{A28}$$

Application of the principle of maximum entropy with constraints (A1), (A2) and (A3) plus the unity integral of the density function will give the density of $\underline{\boldsymbol{z}}$ as:

$$f(\boldsymbol{z}) = \frac{2}{\pi^{5/2}} \left(\frac{1}{a}\right)^2 \left(\frac{7m_0}{4\varepsilon}\right)^{7/2} g \exp\left(-\frac{7m_0}{4\varepsilon}\left(\|\underline{u}\|^2 + 2gx_3\right)\right) \tag{A29}$$

which is again uniform for the location coordinates x_1, x_2, exponential for the location coordinate x_3, and Gaussian for the translational and rotation coordinates. The entropy is then calculated as

$$\Phi[\underline{\boldsymbol{z}}] = \frac{7}{2} \ln\left(\frac{2^{12/7}\pi^{5/7}\mathrm{e}}{7} \frac{m_0^{1/7} I^{2/7}}{g^{2/7} h^{10/7}} \varepsilon a^{4/7}\right) \tag{A30}$$

The marginal distribution of each of the location coordinates $\underline{x}_i$ is easily found to be

$$f_{x_1}(x_1) = f_{x_2}(x_2) = \frac{1}{a}, \qquad 0 \leq x_1, x_2 \leq a, \qquad f_{x_3}(x_3) = \frac{7gm_0}{2\varepsilon} \exp\left(-\frac{7gm_0}{2\varepsilon} x_3\right) \tag{A31}$$

Again, the last equation shows that the density decreases exponentially with altitude. The marginal distribution of each of the velocity coordinates $\underline{u}_i$ is derived as

$$f_{u_i}(u_i) = \left(\frac{7m_0}{4\pi\varepsilon}\right)^{1/2} \exp\left(-\frac{7m_0}{4\varepsilon} u_i^2\right) \tag{A32}$$

This is Gaussian with mean 0 and variance $2\varepsilon/7m_0$.

Once $f(\boldsymbol{z})$ has been determined in equation (A29), the mean energy can be partitioned into thermal and dynamic (due to gravity) as follows:

$$\varepsilon_\theta \coloneqq \mathrm{E}\left[m_0\|\underline{u}\|^2/2\right] = \frac{5\varepsilon}{7}, \qquad \varepsilon_g \coloneqq \mathrm{E}\left[m_0 g \underline{x}_3\right] = \frac{2\varepsilon}{7} \tag{A33}$$

Given that the kinetic state of a diatomic molecule has five degrees of freedom, the above result shows that gravity is equivalent to two additional degrees of freedom. Furthermore, we readily deduce from the above results that the joint distribution $f(\boldsymbol{z})$ is a product of functions of $\boldsymbol{z}$'s coordinates $(x_1, x_2, x_3, u_1, u_2, u_3, u_4, u_5)$. This means that all eight stochastic variables are jointly independent. The independence results from entropy maximization. From (A29) and (A32) we also observe a symmetry with respect to the five kinetic coordinates, resulting in equipartition of the total energy ε into $\varepsilon/7$ for each degree of freedom (*equipartition* principle, a result of entropy maximization).

The mean volume of the column, regarded as a stochastic variable, is

$$\mu_V := \mathrm{E}[\underline{V}] = a^2 \mathrm{E}[\underline{x}_3] = a^2 \int_0^\infty \frac{7gm_0}{2\varepsilon} \exp\left(-\frac{7gm_0}{2\varepsilon} x_3\right) \mathrm{d}x_3 = \frac{2\varepsilon a^2}{7gm_0} \tag{A34}$$

so that, to have constant μ_V the size a should be

$$a = \left(\frac{7gm_0}{2\varepsilon} \mu_V\right)^{1/2} \tag{A35}$$

Equation (A30) can then be written as

$$\Phi[\underline{\boldsymbol{z}}] = \frac{7}{2} \ln\left(\frac{2^{12/7} \pi^{5/7} \mathrm{e}}{5^{5/7} 2^{2/7}} \frac{m_0^{3/7} I^{2/7}}{h^{10/7}} \varepsilon_\theta^{5/7} \mu_V^{2/7}\right) \tag{A36}$$

Taking the derivative with respect to ε_θ, we easily find

$$\frac{1}{\theta} = \frac{\partial \Phi}{\partial \varepsilon_\theta} = \frac{5}{2\varepsilon_\theta} \Rightarrow \theta = \frac{2\varepsilon_\theta}{5} \tag{A37}$$

This has units of energy and to convert it to the thermodynamic temperature T we must divide it by Boltzmann constant ($T = \theta/k$).

The above analysis was made for the entire air column. Next, we will fix the altitude to a specific value x_3 and find the same quantities conditional on this altitude. Using the subscript C for conditional, in this case we have

$$f_{\mathrm{C}}(\boldsymbol{z}|x_3) = \frac{f(\boldsymbol{z})}{f_{x_3}(x_3)} = \left(\frac{1}{a}\right)^2 \left(\frac{7m_0}{4\pi\varepsilon}\right)^{5/2} \exp\left(-\frac{7m_0}{4\varepsilon}\left(\|\underline{u}\|^2\right)\right) \tag{A38}$$

where we observe that the conditional probability density does not depend on the altitude x_3. Now the integration volume is $\Omega_{\mathrm{C}} := \{0 \leq x_{1,2} \leq a, -\infty < u_i < \infty; i = 1, \dots, 5\}$. Integrated over this volume, the mean energy is:

$$\varepsilon_\theta = \mathrm{E}\left[m_0 \|\underline{u}\|^2/2\right] = \int_{\Omega_{\mathrm{C}}} (u_1^2 + u_2^2 + u_3^2 + u_4^2 + u_5^2)\, f_{\mathrm{C}}(\boldsymbol{z}) \mathrm{d}\boldsymbol{z} = \frac{5\varepsilon}{7} \tag{A39}$$

This is the same as in the unconditional case. The potential energy is fixed, $\varepsilon_g = m_0 g x_3$, and its average over the column is

$$\varepsilon_g \coloneqq \int_0^\infty m_0 g x_3 f_{x_3}(x_3)\mathrm{d}x_3 = \frac{2\varepsilon}{7} \tag{A40}$$

in consistence with the previous result.

To calculate entropy in conditional mode, we again assume a fixed cube with edge a centered at the altitude x_3, with $a \ll x_3$, so that a uniform distribution for the location of the molecule in the cube be plausible. In this case, based on the results in Koutsoyiannis (2014) and substituting $5\varepsilon/7$ for ε, we have

$$f_{\mathrm{F}}(\boldsymbol{z}) = \left(\frac{1}{a}\right)^3 \left(\frac{7m_0}{4\pi\varepsilon}\right)^{5/2} \exp\left(-\frac{7m_0}{4\varepsilon}\left(\|\underline{u}\|^2\right)\right) \tag{A41}$$

with the same thermal energy

$$\varepsilon_\theta = \frac{5\varepsilon}{7} \tag{A42}$$

entropy,

$$\Phi_{\mathrm{F}}[\underline{\boldsymbol{z}}] = \frac{5}{2}\ln\left(\frac{4\pi\mathrm{e}}{7}\,\frac{m_0^{3/5} I^{2/5}}{h^2}\,\varepsilon a^{6/5}\right) \tag{A43}$$

and temperature

$$\frac{1}{\theta_{\mathrm{F}}} = \frac{\partial \Phi_{\mathrm{F}}}{\partial \varepsilon} \Big/ \frac{\partial \varepsilon_\theta}{\partial \varepsilon} = \frac{5}{2\varepsilon} \Big/ \frac{5}{7} \Rightarrow \theta_F = \frac{2\varepsilon}{7} = \frac{2\varepsilon_\theta}{5} \tag{A44}$$

which is constant, independent of x_3.

Appendix C: Molecular motion simulation

Simulation setup

We conducted a molecular dynamics simulation to validate the theoretical expectation that, in the absence of convection and radiation, the atmosphere should be isothermal. The simulation software was developed in-house and is available for testing within the Supplementary Information of the paper and at https://www.itia.ntua.gr/2537/. The software architecture follows the principles of event-driven simulations, as described by Pöschel and Schwager (2005).

The system consists of 100 000 particles with a kinetic diameter of 3.64×10^{-10} m and molecular mass of 4.65×10^{-26} kg—parameters closely resembling those of nitrogen molecules. We assume the particles behave as perfectly elastic hard spheres. The simulation box has a size of $L = 1.55 \times 10^{-7}$ m. A gravitational field of –9.8 m/s^2 is applied vertically along the vertical axis ($z \equiv x_3$).

The simulation uses periodic boundary conditions along the horizontal axes ($x \equiv x_1, y \equiv x_2$) and reflective boundaries in the plane perpendicular to the *z*-axis. When a molecule hits the bottom boundary, its vertical velocity component u_z is reversed, while u_x and u_y remain unchanged.

The total initial energy was chosen such that particles rarely reach the top boundary, as seen in the accompanying videos (available within the Supplementary Information of the paper and at https://www.itia.ntua.gr/2537/). Additionally, as seen in Figure A2 (bottom) below, the density at the top 1% part of the simulation box is just 0.00004% of that at the bottom 1% part. Thus, the setup effectively simulates an infinite column with reflective surface, with gas confinement due solely to gravity.

Energy and momentum are conserved in the system. More specifically, the system's total energy (kinetic plus potential) is precisely conserved, while, due to the reflections at the bottom boundary, the total momentum fluctuates, yet it is conserved statistically.

As can be seen in the videos, initially the particles are uniformly distributed up to about 30% of the box height, with small random deviations in *x* and *y* directions. We then allow the system to evolve under gravity until it reaches a steady dynamic state. The simulation runs for 1.2 billion collisions, averaging 24 000 collisions per particle.

Velocity distribution

We periodically sampled velocities along the three axes. As shown in Figure A1, the velocity distribution along the *x* axis closely matches a normal distribution with the same mean and variance. An Anderson-Darling test for normality yielded a statistic of 0.31, indicating that we cannot reject a normality hypothesis (like in the classical 1D Maxwell-Boltzmann form). Same findings hold for the *y* and *z* direction.

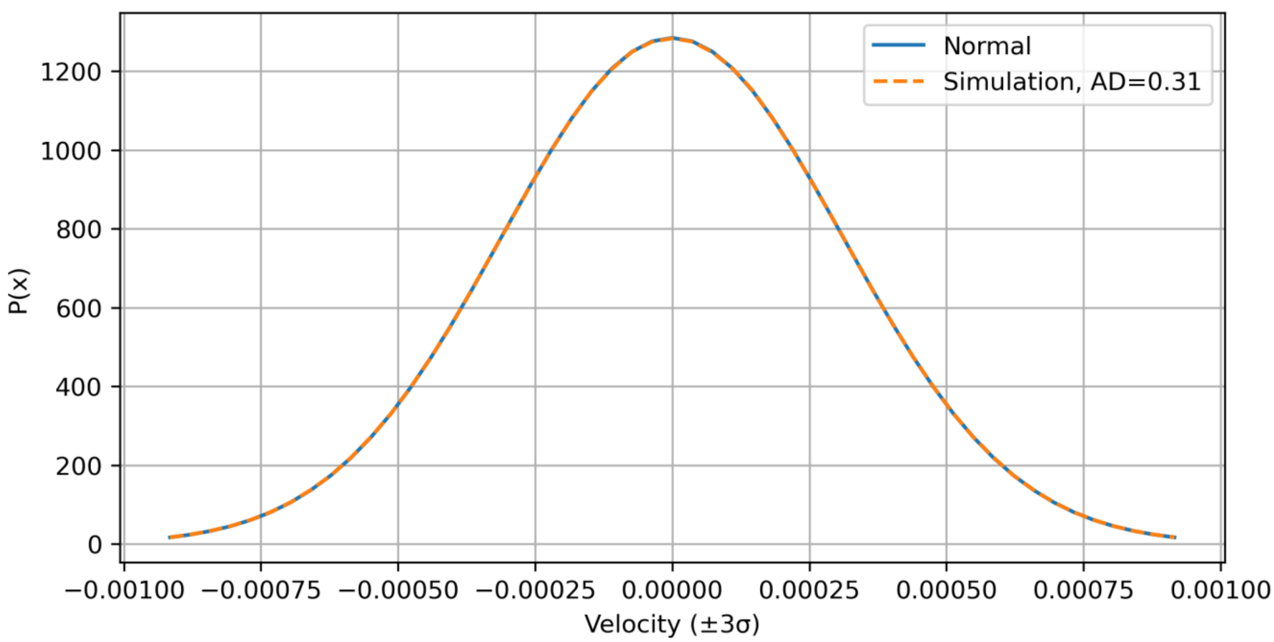

Figure A1 Probability density function of the velocity at the horizontal *x* direction: Simulation data (dashed orange line) and same mean-variance normal distribution (continuous blue line, indistinguishable from the dashed line).

Density and temperature

We divided the simulation domain into 100 horizontal slabs of equal height ($L/100$) from bottom to top. Every 25 000 collisions, we measured the density and temperature in each slab. After completing 1.2 billion collisions (24 000 per particle), we averaged the measurements to generate profiles of density and temperature per height.

Figure A2 shows gas density versus height, where an exponential decrease of density with height is observed (a straight line in a plot on a logarithmic density axis). A non-equilibrium boundary layer (Knudsen layer with typical thickness of a few mean free paths) forms near the bottom, where particle-wall interactions distort local distributions. As seen in the view zoomed at the bottom of the simulation box (right panel), for height $< 0.6\times10^{-9}$, the density distribution is distorted. To exclude this effect from our results, we assumed a transition height further up, at height $\approx10^{-8}$ m. All data from lower slices were excluded and grayed out in the plot.

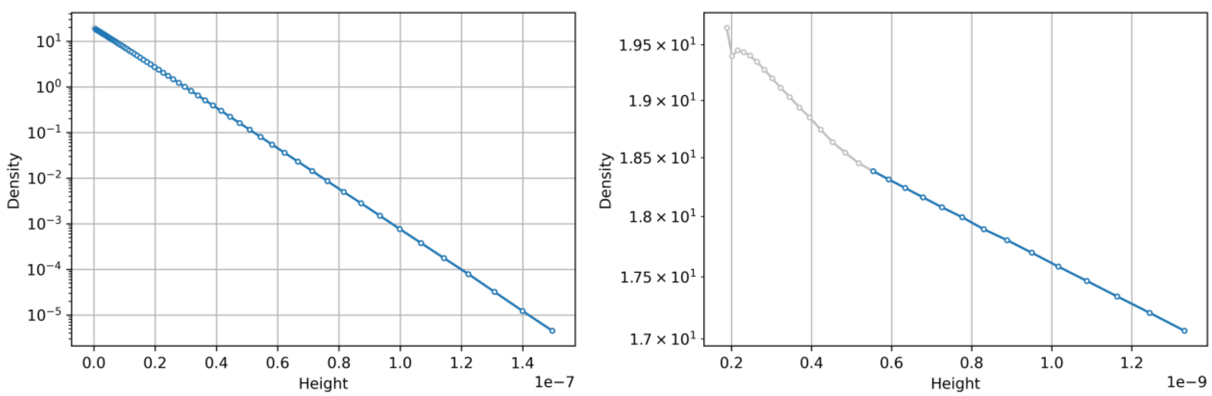

Figure A2 Density measurements per height (logarithmic profile): (**left**) full range of scales; (**right**) zoom at the bottom of the simulation box.

Figure A3 shows the profiles of density and temperature in linear plots. The lowest slab used is at height 1.02×10^{-8} m (determined from Figure A2 as explained), which we treat as the base level (analogous to sea level). Densities and temperatures at all other heights are expressed as percentages of this baseline.

Above a certain level (0.7×10^{-7} m in Figure A2) the temperature fluctuates irregularly, which is a statistical effect due to the small number of particles per slab. Still, below this height (where the density falls to 0.29% of the base) the temperature profile remains remarkably flat. This suggests that the temperature is independent of altitude in this regime. Beyond that, larger fluctuations would require more simulation time for robust conclusions.

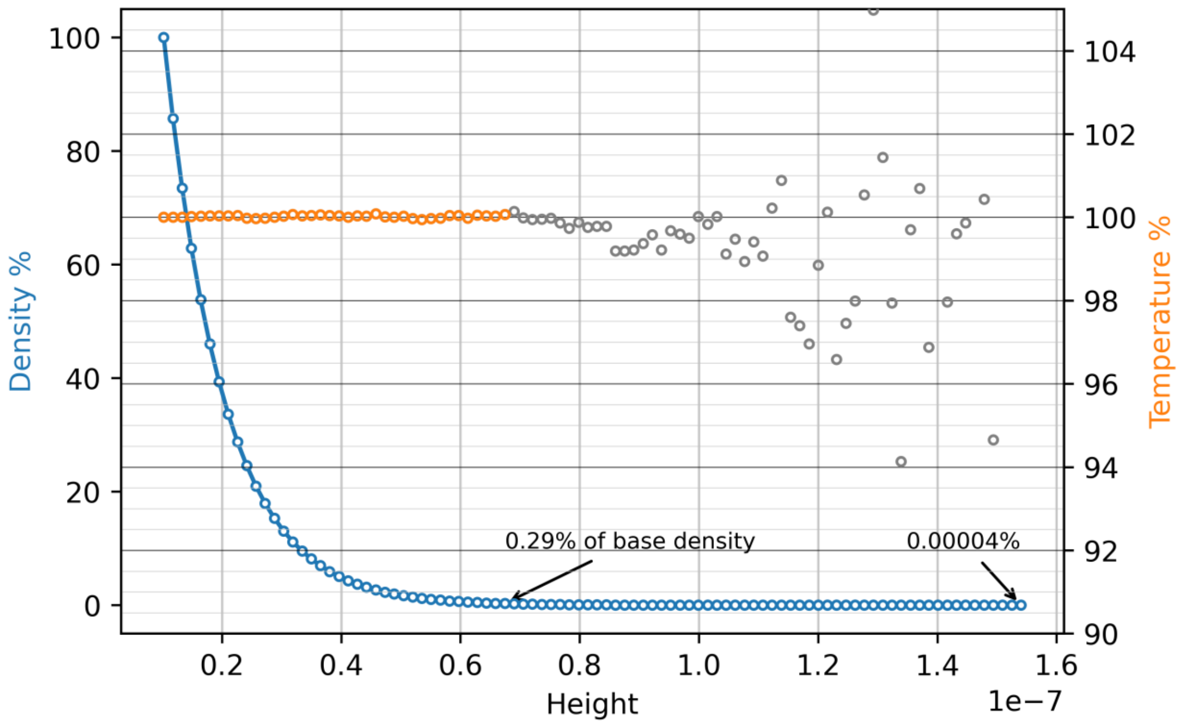

Figure A3 Linear profiles of density and temperature.

To make the simulation results physically realistic, as shown in Figure 3, we made the following conversions (rescaling). We set the base density to 1.2 kg/m³ (sea-level air density) and scale the other values accordingly using the percentages shown in Figure A3. When the density reaches ~30% of the base, we mark it as the top of the troposphere (~10 km). The top of the stratosphere is also annotated in Figure 3. For the temperature, we set the base to 252 K and plot the profile accordingly. As seen, the temperature remains essentially constant throughout the troposphere and stratosphere. Overall, the simulation and analysis support the conclusion that, in the absence of radiation and convection, the atmosphere remains isothermal for all practical purposes.

Conflict of Interest

The authors declare that the research was conducted in the absence of any commercial or financial relationships that could be construed as a potential conflict of interest.

Author Contributions

Conceptualization DK; Data curation DK; Formal analysis DK, GT; Investigation DK, GT; Methodology DK, GT; Project administration DK; Software DK, GT; Supervision DK; Validation DK, GT; Visualization GT; Writing – original draft; DK; Writing – review & editing: DK, GT.

Funding

This research received no funding but was conducted out of scientific curiosity.

Acknowledgments

We are grateful to the colleagues and organizations who have put their huge data sets online along with the data processing and computational systems they have developed. These include the CERES data, the ERA5 Reanalysis, the CLIMEXP and WRIT data and software platforms, and the RRTM software system.

Supplementary Material

Supplementary Material includes the software code of the simulation (C++ and executable) and analysis of its results (Python), files with simulation inputs and outputs, and videos with visualization of simulation. During and after the review phase, all files of Supplementary Material are also publicly available at https://www.itia.ntua.gr/2537/.

Data Availability Statement

All datasets analyzed in this study can be found in the links given in section 2 and the references cited there.

References

Ångström, A., 1915. *A Study of the Radiation of the Atmosphere Based Upon Observations of the Nocturnal Radiation During Expeditions to Algeria and to California*. Smithsonian Miscellaneous Collections, 65 (3), 159 pp., Smithsonian Institution Publication 2354, Washington DC, USA, https://repository.si.edu/handle/10088/23534.

Barth, M.C. and Titus, J.G. eds., 1984. *Greenhouse Effect and Sea Level Rise: A Challenge for This Generation*, Van Nostrand Reinhold, New York, 360 pp., https://archive.org/details/greenhouseeffect0000unse_e4l4/.

Beers, N.R., 1945. Meteorological thermodynamics and atmospheric statics. Sec. V in *Handbook of Meteorology*, edited by F.A. Berry, E. Bollay, and N.R. Beers, McGraw-Hill, New York.

Bernard Jr, H.W., 1980. *Greenhouse Effect*. Ballinger Publishing, Cambridge, Massachusetts, USA, 216 pp. https://archive.org/details/greenhouseeffect0000bern.

Bolin, B., Döös, B.R., Jäger, J. and Warrick, R.A. eds., 1986. *The Greenhouse Effect, Climatic Change and Ecosystems*. Wiley, Chichester, New York, USA, 541-pp, https://archive.org/details/greenhouseeffect00boli/.

Budyko, M.I., 1969. The effect of solar radiation variations on the climate of the Earth. *Tellus*, 21 (5), 611-619.

Budyko, M.I., 1977. *Climatic Changes*. Wiley Waverly Press, Inc. Baltimore, USA (Translation by the American Geophysical Union from the Russian Edition¸ 1974 by Gidrometeoizdat, Leningrad).

CERES, 2021: *CERES_SSF1deg_Hour/Day/Month_Ed4A Data Quality Summary*. Version 2. https://ceres.larc.nasa.gov/documents/DQ_summaries/CERES_SSF1deg_Ed4A_DQS.pdf (Updated 8/4/2023).

Darrigol, O., 2021. Boltzmann's reply to the Loschmidt paradox: a commented translation. *The European Physical Journal H*, 46 (1), 29.

Dimitriadis, P., Koutsoyiannis, D., Iliopoulou, T., and Papanicolaou, P., 2021. A global-scale investigation of stochastic similarities in marginal distribution and dependence structure of key hydrological-cycle processes, *Hydrology*, 8 (2), 59, doi: 10.3390/hydrology8020059.

EXXON, 1982. C*O2 Greenhouse Effect: Technical Review*. EXXON Research and Engineering Company, EC-11-5, Florham Park, New Jersey, USA, 07 9 32, 46 pp., https://archive.org/details/1982ExxonPrimerOnCO2GreenhouseEffect.

Gay, K., 1986. *The Greenhouse Effect*. F. Watts, New York, 104 pp., https://archive.org/details/greenhouseeffect00gayk.

Goessling, H.F., Rackow, T. and Jung, T., 2025. Recent global temperature surge intensified by record-low planetary albedo. *Science*, 387 (6729), 68-73.

Goldman, A., Murcray, F.J., Murcray, F.H., Murcray, D.G. and Rinsland, C.P., 1988. Measurements of several atmospheric gases above the South Pole in December 1986 from high-resolution 3-to 4-μm solar spectra. *Journal of Geophysical Research: Atmospheres*, 93 (D6), 7069-7074.

Goode, P.R., Pallé, E., Shoumko, A., Shoumko, S., Montañes-Rodriguez, P., and Koonin, S.E., 2021. Earth's albedo 1998–2017 as measured from earthshine. *Geophysical Research Letters*, 48, e2021GL094888, doi: 10.1029/2021GL094888.

Gordon, I.E., Rothman, L.S., Hargreaves, E.R., Hashemi, R., Karlovets, E.V., Skinner, F.M., Conway, E.K., Hill, C., Kochanov, R.V., Tan, Y. and Wcisło, P., 2022. The HITRAN2020 molecular spectroscopic database. *Journal of Quantitative Spectroscopy and Radiative Transfer*, 277, 107949.

Gribbin, J., 1982. *Future Weather and the Greenhouse Effect. A Book About Carbon Dioxide, Climate and Mankind*. Delacorte Press/Eleanor Friede/Dell Publishing, New York, NY, USA, 324 pp., https://archive.org/details/futureweathergre0000grib_e7u3/.

Grok 3 beta, Cohler, J., Legates, D., Soon, F., and Soon, W., 2025. A critical reassessment of the anthropogenic CO_2-global warming hypothesis: empirical evidence contradicts IPCC models and solar forcing assumptions, *Science of Climate Change*, 5 (1), 1-16, doi: 10.53234/SCC202501/06.

Hanel, R.A., and Conrath, B.J., 1970. Thermal emission spectra of the earth and atmosphere from the Nimbus 4 Michaelson interferometer experiment, *Nature* 228, 143.

Huber, M., 2008: A hotter greenhouse? *Science*, 321, 353-354.

Huber, B., MacLeod, K.G., and Wing, S.L., 2000. *Warm Climates in Earth History*. Cambridge Press, 462 pp.

ICAO (International Civil Aviation Organization) 1993. *Manual of the ICAO Standard Atmosphere: Extended to 80 Kilometres / 262 500 Feet*. 3rd Ed., Doc 7488/3, ICAO, Montreal, Canada, 304 pp.

Koll, D.D. and Cronin, T.W., 2018. Earth's outgoing longwave radiation linear due to H2O greenhouse effect. *Proceedings of the National Academy of Sciences*, 115 (41), 10293-10298.

Koonin, S.E., 2021. *Unsettled: What Climate Science Tells Us, What It Doesn't, and Why It Matters*. BenBella Books, Dallas, TX, USA.

Koutsoyiannis, D., 2000. *Lecture notes on Hydrometeorology - Part 1*. Edition 2, National Technical University of Athens, Athens, Greece, 157 pp., https://www.itia.ntua.gr/en/docinfo/116/.

Koutsoyiannis, D., 2012. Clausius-Clapeyron equation and saturation vapour pressure: simple theory reconciled with practice. *European Journal of Physics*, 33 (2), 295–305, doi: 10.1088/0143-0807/33/2/295.

Koutsoyiannis, D., 2013. Hydrology and change. *Hydrological Sciences Journal*, 58 (6), 1177–1197, doi: 10.1080/02626667.2013.804626.

Koutsoyiannis, D., 2014. Entropy: from thermodynamics to hydrology. *Entropy*, 16 (3), 1287–1314, doi: 10.3390/e16031287/

Koutsoyiannis, D., 2021. Rethinking climate, climate change, and their relationship with water. *Water*, 13 (6), 849, doi:10.3390/w13060849.

Koutsoyiannis, D., 2024a. *Stochastics of Hydroclimatic Extremes – A Cool Look at Risk*, Edition 4, ISBN: 978-618-85370-0-2, 400 pp., Kallipos Open Academic Editions, Athens, doi: 10.57713/kallipos-1; https://www.itia.ntua.gr/2000/.

Koutsoyiannis, D., 2024b. Relative importance of carbon dioxide and water in the greenhouse effect: Does the tail wag the dog?. *Science of Climate Change*, 4 (2), 36–78, doi: 10.53234/scc202411/01.

Koutsoyiannis, D., 2024c. The relationship between atmospheric temperature and carbon dioxide concentration. *Science of Climate Change*, 4 (3), 39–59, doi: 10.53234/scc202412/15.

Koutsoyiannis, D., and Vournas, C., 2024. Revisiting the greenhouse effect—a hydrological perspective. *Hydrological Sciences Journal*, 69 (2), 151–164, doi: 10.1080/02626667.2023.2287047.

Koutsoyiannis, D., Onof, C., Kundzewicz, Z.W., and Christofides, A., 2023. On hens, eggs, temperatures and CO_2: Causal links in Earth's atmosphere. *Sci*, 5 (3), 35, doi: 10.3390/sci5030035.

Lee, S., 2014. A theory for polar amplification from a general circulation perspective. *Asia-Pacific Journal of Atmospheric Sciences*, 50, 31-43.

Lindzen, R.S., 2020. An oversimplified picture of the climate behavior based on a single process can lead to distorted conclusions. *The European Physical Journal Plus*, 135 (6), 462.

Loschmidt, J. 1876. Über den Zustand des Wärmegleichgewichtes eines Systems von Körpern mit Rücksicht auf die Schwerkraft. *Sitzungsberichte der Akademie der Wissenschaften*, Wien, 73, 128–142.

Ma, N., Zhang, Y., and Yang, Y., 2025. Recent decline in global ocean evaporation due to wind stilling. *Geophysical Research Letters*, 52, e2024GL114256, doi: 10.1029/2024GL114256.

Malik, M., Kempton, E.M.R., Koll, D.D., Mansfield, M., Bean, J.L. and Kite, E., 2019. Analyzing atmospheric temperature profiles and spectra of M dwarf rocky planets. *The Astrophysical Journal*, 886 (2), 142.

McClatchey, R.A., Benedict, W., Clough, S.A., Burch, D.E., Calfee, R.F., Fox, K., Rothman, L.S. and Garing, J.S., 1973. AFCRL atmospheric absorption line parameters compilation. *AFCRL-TR-73-0096, Environmental Research Papers*, No. 434, Optical Physics Laboratory.

Miskolczi, F., 2023. Greenhouse gas theories and observed radiative properties of the Earth's atmosphere, *Science of Climate Change*, 3, 232–289, doi: 10.53234/scc202304/05.

Mlawer, E.J., Taubman, S.J., Brown, P.D., Iacono, M.J. and Clough, S.A., 1997. Radiative transfer for inhomogeneous atmospheres: RRTM, a validated correlated-k model for the longwave. *Journal of Geophysical Research: Atmospheres*, 102 (D14), 16663-16682.

Murray, W. 1979. *The Greenhouse Theory and Climatic Change*. Minister of Supply and Services Canada, Canada Communication Group Publishing, Ottawa, Canada, https://archive.org/details/31761116329905/.

Nikolov N., Zeller K, 2017: New insights on the physical nature of the atmospheric greenhouse effect deduced from an empirical planetary temperature. *Model. Environ. Pollut. Climate Change*, 1, 1000112, doi: 10.4172/2573-458X.1000112.

Nikolov, N. and Zeller, K.F., 2024. Roles of earth's albedo variations and top-of-the-atmosphere energy imbalance in recent warming: New insights from satellite and surface observations. *Geomatics*, 4 (3), 311-341.

O'Connell, P.E. Koutsoyiannis, D., Lins, H.F. Markonis, Y., Montanari, A., and Cohn, T.A., 2016. The scientific legacy of Harold Edwin Hurst (1880 – 1978). *Hydrological Sciences Journal*, 61 (9), 1571–1590, doi: 10.1080/02626667.2015.1125998.

Papoulis, A., 1990. *Probability and Statistics*, Prentice-Hall, New Jersey, USA.

Penman, H.L., 1948. Natural evaporation from open water, bare soil and grass. *Proceedings of the Royal Society of London. Series A. Mathematical and Physical Sciences*, 193 (1032), 120-145.

Pöschel, T., and Schwager, T., 2005. *Computational Granular Dynamics: Models and Algorithms*. Springer, Berlin, Heidelberg, Germany. ISBN 978-3-540-21485-4.

Rothman, L.S., Gamache, R.R., Goldman, A., Brown, L.R., Toth, R.A., Pickett, H.M., Poynter, R.L., Flaud, J.M., Camy-Peyret, C., Barbe, A. and Husson, N., 1987. The HITRAN database: 1986 edition. *Applied Optics*, 26 (19), 4058-4097.

Samuelson, R.E., 1965. Greenhouse Effect in Semi-Infinite Scattering Atmospheres (No. NASA-TM-X-57063), https://archive.org/details/NASA_NTRS_Archive_19670009381.

Sánchez-Lavega, A., Pérez-Hoyos, S. and Hueso, R., 2004. Clouds in planetary atmospheres: A useful application of the Clausius–Clapeyron equation. *American Journal of Physics*, 72 (6), 767-774.

Tyndall, J., 1865. On radiation: Bede lecture. Cambridge University Press, https://archive.org/details/onradiationbede00tyndgoog/.

U.S. House of Representatives, 1984. *Carbon Dioxide and the Greenhouse Effect. Hearing before the Subcommittee on Investigations and Oversight and the Subcommittee on Natural Resources, Agriculture Research and Environment of the Committee on Science and Technology*. U.S. House of Representatives, Ninety-Eighth Congress, Second Session (ERIC ED258833), U.S. Government Printing Office, Washington DC. USA, 205 pp., https://archive.org/details/ERIC_ED258833.

U.S. Standard Atmosphere, 1976, U.S. Government Printing Office, Washington, DC, USA, https://www.ngdc.noaa.gov/stp/space-weather/online-publications/miscellaneous/us-standard-atmosphere-1976/us-standard-atmosphere_st76-1562_noaa.pdf.

van Wijngaarden, W.A. and Happer, W., 2023. Atmosphere and Greenhouse Gas Primer. arXiv preprint, arXiv:2303.00808, https://arxiv.org/abs/2303.00808.

van Wijngaarden, W.A. and Happer, W., 2025. Radiation transport in clouds, *Science of Climate Change*, 5 (1), 1-12, doi: 10.53234/scc202501/02.

Wiencke, B., 2021. A proposed new model for the prediction of latitude-dependent atmospheric pressures at altitude. *Science and Technology for the Built Environment*, 27 (9), 1221-1242.

Wildt, R., 1965. *The Greenhouse Effect in a Gray Planetary Atmosphere* (No. NASA-TM-X-56621). https://archive.org/details/NASA_NTRS_Archive_19660012929 .